the plant journal

SEB SOCIETY FOR EXPERIMENTAL BIOLOGY

The Plant Journal (2025) **122,** e70139 doi: 10.1111/tpj.70139

Topologically associating domains and the evolution of three-dimensional genome architecture in rice

Amina Kurbidaeva[1], Sonal Gupta[1,2], Maricris Zaidem[1,3], Raúl Castanera[4,5], Yutaka Sato[6], Zoé Joly-Lopez[1,7], Josep M. Casacuberta[4] and Michael D. Purugganan[1,8,*]

[1]*Center for Genomics and Systems Biology, New York University, New York, New York 10003, USA,*
[2]*Trivedi School of Bioscience, Ashoka University, Sonipat, India,*
[3]*Department of Biology, University of Oxford, Oxford, UK,*
[4]*Centre for Research in Agricultural Genomics, Cerdanyola del Vallès, Barcelona, Spain,*
[5]*IRTA, Genomics and Biotechnology, Edifici CRAG, Campus UAB, Bellaterra, Catalonia 08193, Spain,*
[6]*National Institute of Genetics, Mishima, Japan,*
[7]*Département de Chimie, Université du Quebéc à Montréal, Montreal, Quebec, Canada, and*
[8]*Center for Genomics and Systems Biology, New York University Abu Dhabi, Abu Dhabi, United Arab Emirates*

Received 10 November 2024; revised 17 February 2025; accepted 25 March 2025.
*For correspondence (e-mail mp132@nyu.edu).

SUMMARY

We examined the nature and evolution of three-dimensional (3D) genome conformation, including topologically associating domains (TADs), in five genomes within the genus *Oryza*. These included three varieties from subspecies within domesticated Asian rice *O. sativa* as well as their closely related wild relatives *O. rufipogon* and *O. meridionalis*. We used the high-resolution chromosome conformation capture technique Micro-C, which we modified for use in rice. Our analysis of rice TADs shows that TAD boundaries have high transcriptional activity, low methylation levels, low transposable element (TE) content, and increased gene density. We also find a significant correlation of expression levels for genes within TADs, suggesting that they do function as genomic domains with shared regulatory features. Our findings indicate that animal and plant TADs may share more commonalities than were initially thought, as evidenced by similar genetic and epigenetic signatures associated with TADs and boundaries. To examine 3D genome divergence, we employed a computer vision-based algorithm for the comparison of chromatin contact maps and complemented this analysis by assessing the evolutionary conservation of individual TADs and their boundaries. We conclude that overall chromatin organization is conserved in rice, and 3D structural divergence correlates with evolutionary distance between genomes. We also note that individual TADs are not well conserved, even at short evolutionary timescales.

Keywords: topologically associating domains, chromosome conformation capture, Micro-C, epigenetics, gene expression, chromatin marks, methylation.

INTRODUCTION

In recent years, researchers have begun to explore the nature of three-dimensional (3D) genome organization (Bouwman & de Laat, 2015; Doğan & Liu, 2018; Dong, Tu, Liang, et al., 2020), which affects gene regulation (Dekker & Heard, 2015; Nora et al., 2012; Ramírez et al., 2018; Zhan et al., 2017) and may play a central role in the evolution of genomic architecture (Farré et al., 2015). The study of higher order structures has been facilitated by advances in chromosome conformation capture (3C) techniques, which have led to the development of methods such as Hi-C (Lieberman-Aiden et al., 2009), Omni-C, and Micro-C (Hsieh et al., 2015), allowing the genome-wide mapping of 3D genome organization. These molecular approaches have enabled the discovery of large chromatin structural elements, such as A/B compartments, as well as smaller self-interacting regions of chromosomes referred to as topologically associating domains (TADs), which are kilo- to megabase-sized genomic regions that interact within the nucleus and are believed to represent a fundamental structural/functional unit of the genome. TADs appear to play a prominent role in gene regulation (Dekker & Heard, 2015) and in genome replication by synchronizing origins of replication (Dang et al., 2023; Eser et al., 2017).

Enhancers that regulate gene expression in regulatory domains are associated with the presence of TADs (Dekker & Heard, 2015), and genes located within the same TAD have been found to have correlated expression patterns (Nora et al., 2012; Ramírez et al., 2018; Zhan et al., 2017). Moreover, TAD boundaries often coincide with breakpoints of chromosomal rearrangements in mammals and fruit flies (Lazar et al., 2018; Liao et al., 2021), leading to the hypothesis that TADs are maintained during evolution as intact units.

In mammals, TADs are thought to be formed by the cohesion–CTCF-mediated loop extrusion mechanism (Fudenberg et al., 2016), whereas in fruit flies other mechanisms have been proposed, including boundary pairing (Bing et al., 2024) and chromatin compartmentalization driven by phase separation (Nuebler et al., 2018). These TADs are delimited by TAD boundaries, which in animals are chromatin accessible regions enriched for active transcription marks and housekeeping genes (Szabo et al., 2018). In mammals, these boundaries bind CCCTC-binding factor (CTCF), and in fruit flies by various insulator proteins including BEAF-32, Chromator, CP190, or M1BP (Szabo et al., 2018).

In plants, there is no consensus on the nature and nomenclature of these interacting chromosomal regions. Certain studies refer to these interacting sequences as chromatin domains (CDs) (Sun et al., 2024), chromatin folding domains (Liao et al., 2022), TAD-like domains (Dong, Tu, Liang, et al., 2020; Grob & Grossniklaus, 2017; Junaid et al., 2023), or more conventionally TADs (Liu et al., 2017). We will refer to such domains as TADs. Until recently, it was thought that TADs exist only in plants with genomes larger than 400 Mb, such as maize (Rowley et al., 2017; Tourdot & Grob, 2023). However, the application of high-resolution Hi-C and Micro-C technologies for plant genomes has shown that plants with small genomes, such as Arabidopsis, also possess TAD-like domains, albeit smaller (Sun et al., 2024; Yin et al., 2023). Evidence has begun to accumulate that plant TADs might also play a functional role in gene regulation; for example, clusters of co-expressed biosynthetic pathway genes in different plants, including rice, are co-localized within TADs (Nützmann et al., 2020). Despite the presence of these genomic features, however, plants do not have the CTCF proteins associated with TAD boundaries in animals, although they do have cohesins (Zhang & Wang, 2021).

Genome studies have indicated that TADs may be conserved functional building blocks of the genome, since rearrangement breakpoints typically observed between species do not typically disrupt TADs (Lazar et al., 2018; Liao et al., 2021, 2022). Evolutionary TAD conservation is important for the preservation of *cis*-regulatory environments necessary for the control of gene expression, which suggests that TAD reorganization may be important for the evolution of novel traits. In the bobtail squid *E. scolopes*, for example, conserved gene neighborhoods involved in the origin of cephalopod-specific traits are located within TADs (Schmidbaur et al., 2022). TAD boundaries, however, paradoxically have a dual nature. On the one hand, these boundaries appear to be evolutionarily constrained (Junaid et al., 2023; McArthur & Capra, 2021) and their deletion is rare and under negative selection (Fudenberg & Pollard, 2019; Huynh & Hormozdiari, 2019). Nevertheless, synteny breakpoints in flies and mammals (Krefting et al., 2018; Lazar et al., 2018) are also enriched at boundaries. Thus, TAD boundaries are conserved elements that preserve gene regulation within specific domains, yet they are prone to be sites of chromosomal breakage, highlighting their role in genome rearrangements during evolution (James et al., 2024).

It is thus unclear the degree to which TADs and their boundaries evolve. For example, a number of direct comparisons of TADs between species have shown that they are strongly conserved in some phylogenies (e.g., mammals) (Vietri Rudan et al., 2015). In contrast, very little conservation of mammalian TAD boundaries was found in a recent study, with only 14% of human boundaries conserved between four primate and four rodent species (Okhovat et al., 2023). More recent studies similarly present contrasting results: for example, only 43% of TADs were found to be conserved between humans and chimpanzees (Eres et al., 2019). Dixon et al. (2012) reported that 76% of mouse TAD boundaries are conserved in humans, although a careful re-evaluation of their data concluded that only 31% of boundaries were conserved between the species (Eres & Gilad, 2021), and other studies indicate that TADs were generally not conserved (Eres et al., 2019). A possible explanation for these contrasting results was suggested by Torosin et al. (2020), who proposed that different types of TADs evolve under different evolutionary forces, with highly conserved TADs in vertebrates and flies enriched for developmentally regulated genes, while TADs enriched for broadly expressed genes evolve rapidly (Harmston et al., 2017; Torosin et al., 2020).

Like animals, plants appear to have varying levels of TAD conservation. Only 8.23% of the foxtail millet domains were conserved in sorghum, and similar results were found in a sorghum and maize comparison (Dong et al., 2017). At the species level, 25% of TADs were found to be conserved between *Brassica rapa* and *Brassica oleracea* (Xie et al., 2019), and 40–48% of TADs were found to be conserved between two poplar species (Zhang, Zhao, et al., 2021). However, these studies assessed TAD conservation at different map resolutions and used different definitions of TAD conservation, which prevents us from generalizing about the overall level of TAD conservation in plants.

To explore the nature and evolution of plant TADs, we investigated the patterns of global 3D genome evolution in domesticated Asian rice (*Oryza sativa*) and two of its

closest wild relatives (*O. rufipogon* and *O. meridionalis*). Unlike most other studies, we chose species/subspecies that have evolved over a relatively recent timescale. Rice was initially domesticated in China from *O. rufipogon* around 9000 years ago as *O. sativa* ssp. *japonica*, which eventually evolved about 4000 years ago into temperate and tropical *japonica*. A separate domestication of rice occurred in the Indian subcontinent ~4500 years ago, leading to *O. sativa* ssp. *indica*, which traces its ancestry to *O. nivara* and diverged from the *japonica* lineage ~550 000 years ago. *O. meridionalis* is the most basal species in the AA group of the genus *Oryza* and diverged from *O. sativa* and *O. rufipogon* ~2.4 million years ago (Stein et al., 2018). Applying the Micro-C method (Hsieh et al., 2015) to these species/subspecies, we show that TADs do appear to be functional units of the rice genome and use gene expression, genomic, and epigenomic data to identify signatures associated with TAD boundaries. Our investigation also examines 3D genome conservation and evolution in closely related *Oryza* genomes and provides insights into chromatin conformation patterns at different scales, showing that global 3D genome evolution closely tracks sequence evolution. Finally, we suggest that while higher-order chromosome organization tracks genome sequence evolution, individual TADs can evolve rapidly.

RESULTS AND DISCUSSION

Generating Micro-C chromatin contact maps of five rice genomes

We first generated high-resolution chromatin contact maps from five *Oryza* genomes. We selected three varieties of domesticated rice *Oryza sativa* that represent the two main subspecies, *indica* (IR64) and *japonica*; for the latter, we used a tropical *japonica* (Azucena) and a temperate *japonica* (Nipponbare). We also worked with two wild species – *O. rufipogon*, the wild ancestor of domesticated *japonica*, and *O. meridionalis* (Figure 1b). To generate these contact maps, we applied the recently developed Micro-C technology (Hsieh et al., 2015), which is a modification of Hi-C that includes a micrococcal nuclease (MNase) digestion step to assess proximity between chromosomal regions. We adapted a Micro-C protocol for use in rice that bypasses nuclei extraction prior to cross-linking and proximity ligation, allowing for faster generation of sequencing data (see "Methods" section).

We assessed the reproducibility of the maps obtained by comparing two biological replicates for each genome (Yang et al., 2017). The replicates showed good concordance (see "Methods" section), and we merged the replicates to obtain high-resolution genome contact maps. We used the definition of Rao et al. (2014) to estimate maximum contact map resolution with HiCRes (Marchal et al., 2022), which was close to 1 kb for all genomes except for *O. meridionalis*, for which we obtained a resolution of 4 kb (Table S1).

The merged chromatin contact maps for the five genomes are shown in Figure 1(a,c). Visual inspection allowed us to observe similar chromosome structures between genomes at low resolution, with contact density strongly concentrated along the main diagonals. Distance-dependent interaction frequencies represented as probability versus distance [$P(s)$] curves (Xu et al., 2021) reveal that intra-chromosomal contact frequencies decay rapidly as genomic distance increases (Figure S1). Overall, we conclude that the Micro-C maps we generated closely align with the reported overall chromosome structure of rice, and we are able to distinguish chromosome territories, compartments, TADs, and loops (Figure 1a). In accordance with previous Hi-C maps of the rice genome (Dong et al., 2017; Liu et al., 2017; Zhao et al., 2019; Zhou et al., 2019), we also found weak intra- and inter-chromosomal clustering of telomeres, represented as off-diagonal areas of higher contact frequencies (Figure 1a). However, no clustering of centromeres was observed, and like others, we conclude that rice chromosomes do not adopt a Rabl conformation characterized by telomeres and centromeres clustering at opposite poles of the nucleus. This is in line with previous cytological (Dong & Jiang, 1998; Prieto et al., 2004) and Hi-C studies (Dong et al., 2017; Liu et al., 2017; Zhao et al., 2019; Zhou et al., 2019).

Identification of TADs from Azucena Micro-C data

To gain insight into the nature of TADs in the rice genome, we decided to dissect the genome of the Azucena rice variety and annotate TADs at high resolution. We chose Azucena given that, as a tropical *japonica*, it may represent the oldest lineage of domesticated rice, and it has been used in multiple functional genomic and systems biology studies (Groen et al., 2020, 2022; Joly-Lopez et al., 2020).

We initially employed three widely used tools for TAD annotation [HiCExplorer (Ramírez et al., 2018), Arrowhead (Rao et al., 2014), and HiTAD (Wang et al., 2017)] to call TADs at three resolutions (1, 2, and 5 kb). All tools clearly identified TAD-like structures, although we observed considerable variation in TAD calls between the tools (Table S2). TADs called by HiCExplorer and HiTAD showed better concordance in TAD number and size. We identified 4650, 6420, and 3630 HiCExplorer domains with a median TAD size of 52, 48, and 75 kb, while using HiTAD, we found 868, 6535, and 3534 domains with a median TAD size of 177, 40, and 70 kb at 1, 2, and 5 kb resolutions, respectively. We therefore decided to proceed with these two tools. To validate the TAD calls from these tools, we also took advantage of the fact that TAD boundaries are enriched for active chromatin marks and depleted for repressive chromatin marks and DNA methylation in

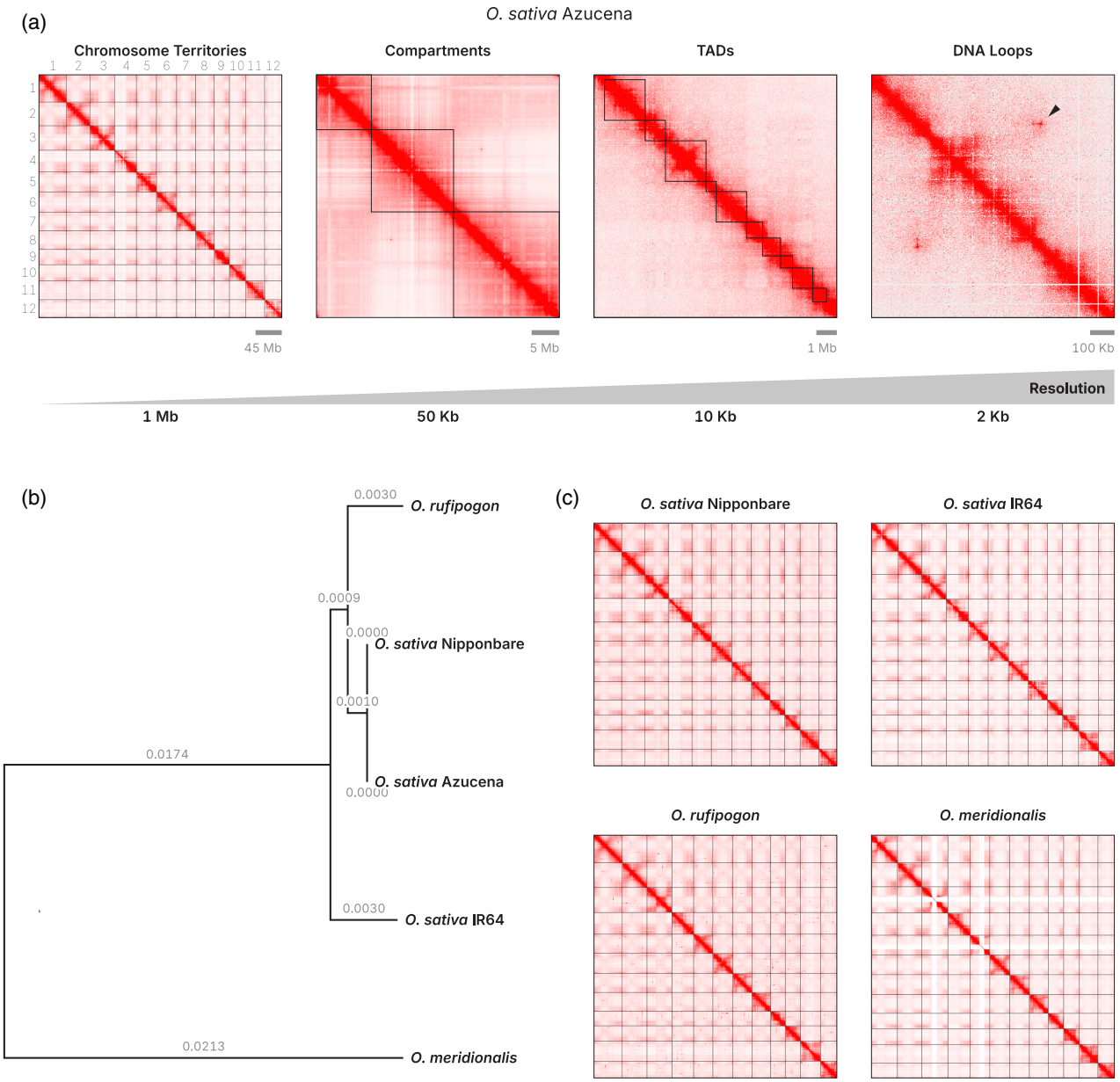

Figure 1. Micro-C analysis of chromatin interactions in rice.
(a) Micro-C contact map of *O. sativa* Azucena variety at different resolutions allows for the detection of various features of the 3D genome. The arrow in the rightmost map shows features associated with loops.
(b) Neighbor-joining tree of the selected *Oryza* genomes created using synonymous site substitutions (dS). Branch labels represent the synonymous substitution rate; estimated divergence times were obtained from Stein et al. (2018).
(c) Genome-wide Micro-C contact maps of rice genomes. Maps are colored according to contact frequencies between bins, with darker red representing more contacts. Lines bounding the 12 chromosomes are shown, with chromosome 1 in the upper left and the numbering proceeding to the right and down, up to chromosome 12.

different organisms, including rice (Dixon et al., 2012; Dong et al., 2017; Hisanaga et al., 2023; Junaid et al., 2023; Liu et al., 2017) (see below). Based on these criteria, we concluded that HiCExplorer accurately called TADs at 1, 2, and 5 kb resolution, whereas HiTAD accurately called TADs only at 2 and 5 kb resolution (see "Methods" section).

The discrepancies in the number and locations of TADs identified by different callers in the same sample and same experiment have been extensively reported in the 3D genomics literature (Liu et al., 2022; Zufferey et al., 2018). There are three major potential explanations for these discrepancies: different algorithmic approaches, various

parameter settings, and the presence of hierarchical TAD structures: To identify a robust set of TADs, we decided to devise an approach based on using TAD callers that employ different algorithms and hierarchical/non-hierarchical approaches. HiCExplorer relies on calculating insulation scores for calling TADs, while HiTAD uses a directionality index (DI) and considers hierarchical TADs. The insulation score measures the number of interactions spanning a given genomic region, while DI assesses the shift in the directionality of contacts upstream and downstream of a region. While strong DI values are a signature of a TAD boundary, they can be associated with many regions in the genome (Gorkin et al., 2019), and we reasoned that TADs called by both methods would represent the most robust set of domains. We therefore identified TADs called by both HiCExplorer and HiTAD tools, with the criteria that the TAD body must reciprocally overlap by at least 80% between both tools (Figure 2a,b). With these criteria, we obtained 2474 TADs at 2 kb resolution. These TADs had a median size of 44 kb and a median number of five genes per TAD, covering 32.3% of the genome (Figure 2c,e,g). At 5 kb resolution, we identified 1207 TADs with a median size of 65 kb, a median number of seven genes per TAD, covering 23.6% of the genome (Figure 2d,f,h). The TADs called at 5 kb resolution had a higher median number of genes per TAD, and since we wanted to analyze gene expression within TADs (see below), we chose the 5 kb resolution dataset for further analysis to increase the power.

In plant and animal genomes, A and B compartments are genomic regions characterized by similar chromosomal features and interaction patterns. A compartments have been shown to contain mainly euchromatin, while B compartments contain mainly heterochromatin (Dong et al., 2017, 2018). To characterize the distribution of TADs between euchromatic and heterochromatic regions of the genome, we first identified the corresponding regions by calling compartments. We did that at the 160 kb resolution using the fanc compartments tool of the FAN-C package (Kruse et al., 2020). Compartment calling was done based on the GC content, where regions with low GC content corresponded to the B compartment, and regions with high GC content corresponded to the A compartments. We then analyzed the relative distribution of TADs between A and B compartments by using the Chi-squared test to compare the observed and expected number of TADs in compartments. The results suggested no strong compartmentalization bias for TADs in terms of association with euchromatin and heterochromatin.

Epigenetic and genetic properties of TADs and TAD boundaries

We wanted to better characterize genomic features associated with TADs and TAD boundaries in Azucena (Figure 3a) and created genome-wide profile plots for a set of genetic and epigenetic features (Joly-Lopez et al., 2020) for these TAD regions (see "Methods" section) (Figure 3b). We found that boundaries of TADs called at 5 kb resolution are enriched in the active promoter-associated marks H3K27ac and H3K4me3. These histone marks play similar roles in metazoans and were previously found to be associated with TAD boundaries in different organisms (Dixon et al., 2012; Dong et al., 2017; Wang et al., 2018). The repressive epigenetic mark H3K27me3 was found to be neither enriched nor depleted at TAD boundaries, consistent with previous findings in pepper (Liao et al., 2022) and cotton (Wang et al., 2018) and in contrast to *Drosophila* boundaries (Liao et al., 2021). Despite it being a repressive mark, it is found at the promoters of 'bivalent' genes, where both H3K27me3 and H3K4me3 mark the transcription start site and is also observed at the promoter of genes associated with active transcription (Young et al., 2011; Zhao et al., 2020). This suggests a complex relationship between boundaries and H3K27me3 enrichment. H3K18ac is a mark associated with enhancers in *Drosophila* (Fedoseeva et al., 2018). We found H3K18ac to be depleted at boundaries, which seem to be associated with promoters and not enhancers; this is, to our knowledge, the first report of the H3K18ac pattern around plant TAD boundaries. We also find that TAD boundaries are enriched with active transcription signals as measured by precision nuclear run-on and sequencing (PRO-Seq), which maps transcriptionally engaged polymerase activity at base-pair resolution. Finally, we observe a depletion for transposable elements (TEs) at TAD boundaries (Figure 3b).

We found that boundaries are associated with higher gene density and lower DNA methylation (Figure 3b). To quantify the differences in gene coverage, we first classified the genome into three categories – TAD boundary (5 kb segments as above, abbreviated as TAD_{br}), TAD body (TAD_{body}, TAD domains identified above minus the TAD_{br} overlap), and non-TAD body (non-TAD_{body}, genomic regions not identified as a TAD_{br} or a TAD_{body}) (Figure S2a). We found that TAD boundaries are enriched for protein-coding genes, whereas there was no difference between TAD_{body} and non-TAD_{body} (Figure 3c). This is consistent with previous findings in rice, which found TAD boundaries have higher gene density, but contrasts with the claim that TADs are depleted for protein-coding genes (Liu et al., 2017). This disparity could be due to their measure of gene density, which was defined as the fraction of chromatin annotated as protein-coding genes, which can be confounded by the length of genes or transcripts. Indeed, we found a significant number of shorter gene transcripts in TAD boundaries (Figure 3d).

Gene and genomic GC content was significantly higher within TAD boundaries (Figure 3e; Figure S2b); this is not surprising given the high gene density in TAD

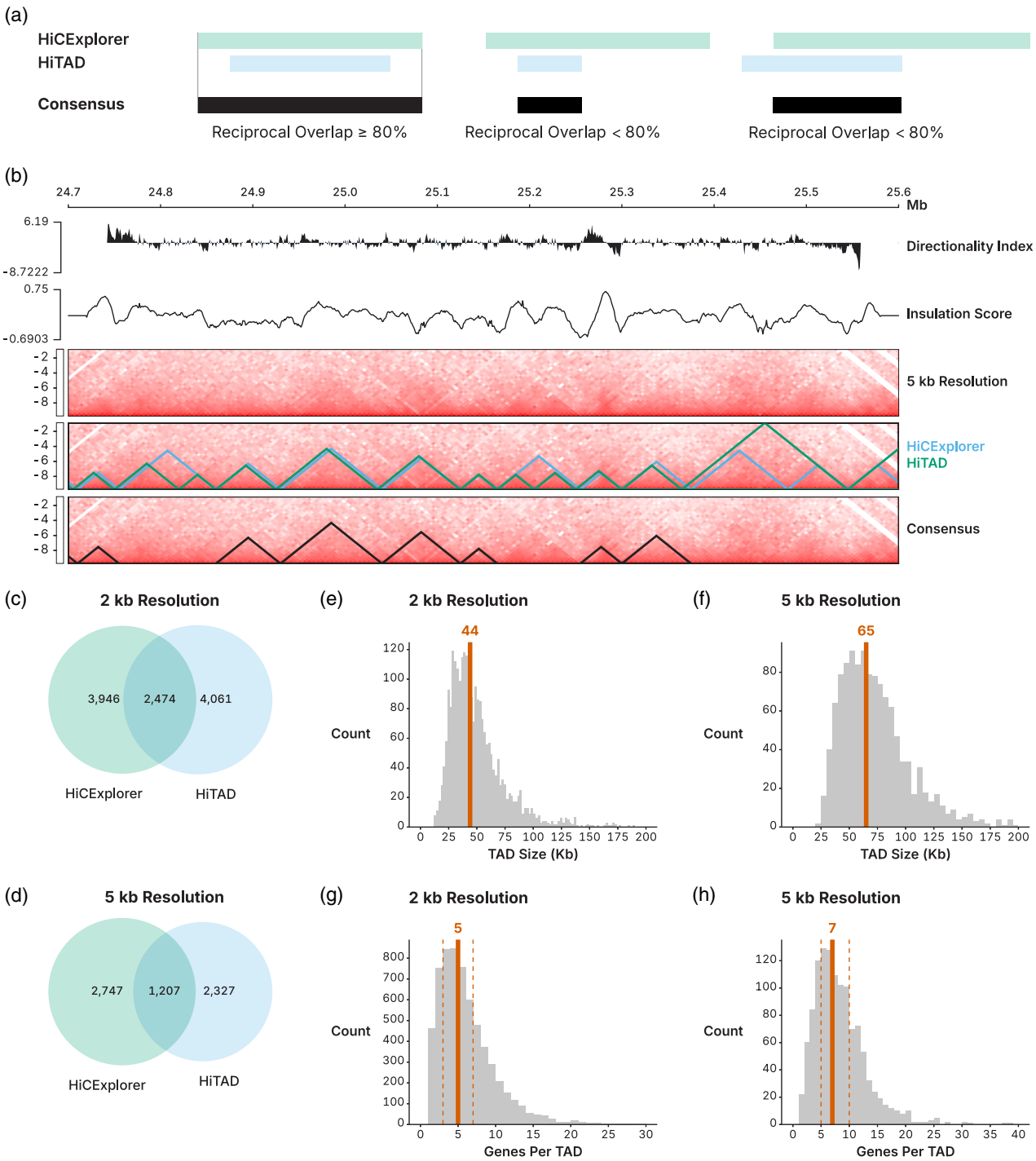

Figure 2. TAD identification from Azucena Micro-C data.
(a) The approach used to call TADs using the two tools HiCExplorer and HiTAD. A TAD call is arrived at by consensus if the reciprocal overlap between the TADs called by the two methods is >80%. The TAD body and boundaries identified by HiCExplorer were retained as the consensus.
(b) An example of an ~1-Mb region of Azucena chromosome 1 with TADs called by the two tools independently, and with the approach depicted in the previous panel. Position in the region is indicated by the numbers above. The directionality index values and the insulation scores are indicated. Contact map resolution is 5 kb.
(c, d) Overlap of TADs called with HiCExplorer and HiTAD tools at 2 and 5 kb resolutions, respectively.
(e, f) Size distribution of Azucena TADs at 2 and 5 kb resolutions, respectively. The median TAD sizes in kb are indicated.
(g, h) Distribution of the number of genes per TAD called at 5 and 2 kb resolutions, respectively. The median gene number per TAD is indicated.

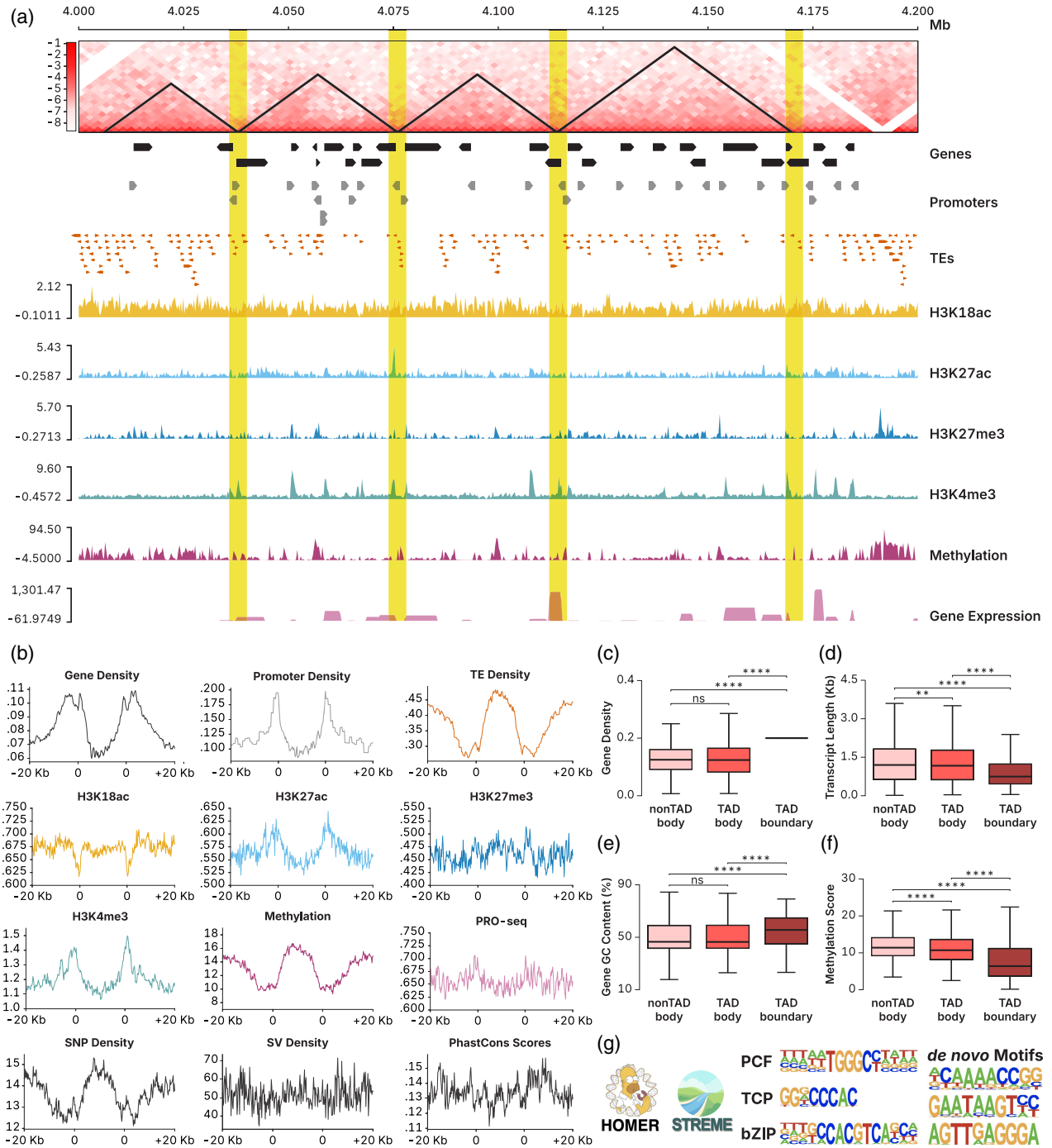

Figure 3. Genetic and epigenetic properties of TADs and TAD boundaries in Azucena.
(a) A representative example of TADs in a 200-kb region on chromosome 1 in Azucena. The panels below show genomic and epigenomic feature distribution. TAD boundaries are highlighted. Genes, promoters and TEs are indicated by thick arrows on top.
(b) Distribution of genomic and epigenomic features across TADs called at 5 kb resolution. TADs were linearly transformed to align the panel's borders. TAD boundaries are marked as '0', and the plots span 20 kb proximal and distal to the boundaries. *X*-axis represent average enrichment per 500 bp.
(c) Gene density, defined as the number of genes within a feature normalized by the length of the feature.
(d) Transcript length in kilobases (kb).
(e) Gene GC content.
(f) Methylation score normalized by the length of the feature, among three classes of genomic regions: TAD body, 5 kb TAD boundary, and non-TAD body (segments of genome not recognized as TAD or boundary). Significance of two-tailed *t*-test depicted as ns, non-significant; $^{**}P < 0.01$, and $^{****}P < 0.0001$.
(g) Sequence motifs enriched at rice TAD boundaries, as detected by HOMER and STREME.

boundaries and that genes have high GC content compared to intergenic regions (Ferguson et al., 2013). We also found that TAD boundaries have lower methylation levels compared to TAD bodies and non-TAD bodies (Figure 3f). All of this taken together indicates that TAD formation in rice may be linked to a high density of short genes with high GC content and low DNA methylation levels.

Lastly, in *Drosophila*, the majority of TAD boundaries identified at high resolution (77%) co-localize with promoters, and those boundaries tend to be flanked by divergently oriented gene promoters (Ramírez et al., 2018). We wanted to see if a similar phenomenon exists in the rice genome. We observed that in our set of boundaries identified at 5 kb resolution, 54.5% overlap with promoters, which is more than would be expected by chance ($P < 2.74 \times 10^{-121}$, binomial test). However, we did not observe an orientation preference for gene promoters flanking rice boundaries, as observed in *Drosophila*. We also found through GO term analysis that genes overlapping TAD boundaries are significantly enriched for genes linked to translation and molecular functions such as RNA binding and ribosome-associated categories (Figure S3). These are typically highly expressed housekeeping genes, which correlates with the fact that boundaries are enriched with active transcription signatures and have low methylation levels, which is consistent with previous work in rice (Liu et al., 2017) and other plant species (Jia et al., 2021; Junaid et al., 2023; Lee & Seo, 2023; Liao et al., 2022; Pei et al., 2022; Tian et al., 2021; Wang et al., 2021; Zhang, Pandey, et al., 2021; Zhang, Zhao, et al., 2021), as well as fungi (Torres et al., 2024), insects (Ramírez et al., 2018), and vertebrates (Li et al., 2022); this suggests common principles governing 3D genome conformation across both plants and animals.

Given the structural and functional role of TADs, it is plausible that their boundaries could be evolutionarily conserved at the sequence level. Indeed, studies show that TAD boundaries are depleted for SNPs in mammals (Fudenberg & Pollard, 2019) and in plants (Liao et al., 2022). However, a previous study in rice did not find a decrease in sequence variation at TAD boundaries, but a dip ~5 kb before boundaries was observed (Golicz et al., 2020). We asked whether SNP density is lower at boundaries in our dataset and used publicly available data from the Rice SNP-Seek Database (Mansueto et al., 2017) which combines variant data from a large panel of rice varieties. We observe a clear reduction of SNP density at boundaries called at 5 kb resolution (Figure 3b), suggesting that rice TAD boundaries are depleted for genomic variation. The differences observed between our and previously published data could be due to different TAD annotation methods used [Armatus in previous study (Golicz et al., 2020) and HiTAD/HiCExplorer in our study].

A number of studies provide evidence for selection against structural variations (SVs) at TAD boundaries in different species, including human (Fudenberg & Pollard, 2019), pepper, tomato (Liao et al., 2022), soybean (Ni et al., 2023), and cotton (Long et al., 2021) genomes. We used the data from Rice SNP-Seek Database (Mansueto et al., 2017) to look at possible SV breakpoint enrichment at TAD boundaries. However, we did not observe differences in the enrichment of structural variant breakpoints around TADs and their boundaries (Figure 3b).

TAD boundaries are enriched for specific DNA motifs

Studies in rice and Arabidopsis have identified that TAD boundaries are enriched in motifs recognized by TCP and bZIP transcription factors (Doğan & Liu, 2018; Liu et al., 2017; Yin et al., 2023). Similarly, in maize, motifs for TCP, AP2-EREBP, and LBD transcription factor binding were proposed to be involved in TAD boundary formation (Tourdot & Grob, 2023). Whether these are associated with actual protein binding is debatable; however, as it has been shown that TCP proteins are not required for TAD boundary formation in *Marchantia polymorpha* despite these boundaries being enriched in TCP binding sites (Karaaslan et al., 2020).

Nevertheless, we searched for boundary protein candidates in our high-resolution rice TAD dataset by performing motif enrichment analysis in TAD boundaries identified at 5 and at 2 kb resolution, using randomly chosen non-boundary sequences as background. Using HOMER (Heinz et al., 2010) and STREME (Bailey, 2021), we observed an enrichment of TCP and bZIP binding motifs in the boundary sequences. Of particular interest were binding motifs of the TCP family PCF proteins, which are a group of seven proteins in rice involved in regulating the expression of genes related to cell division, growth, and differentiation, and associated with drought and salt tolerance (Kosugi & Ohashi, 2002). These proteins tend to form homo- and/or heterodimers between members of the same class (Kosugi & Ohashi, 2002), similar to proteins involved in TAD boundary formation in metazoans (Bonchuk et al., 2015; Bouwman & de Laat, 2015), and may be candidates for boundary proteins in rice. Finally, in addition to these known motifs, we also identified three *de novo* motifs enriched at rice TAD boundaries (Figure 3g).

TADs are gene expression regulatory units

The idea that TADs represent not only structural, but also functional genomic units, finds support in several observations made in animals. In mammals, histone modifications are often similar within genes of the same TAD (Nora et al., 2012; Rao et al., 2014). In addition, genes within the same TADs change their expression during cell differentiation in a similar way (Nora et al., 2012), and co-regulated genes often are located within a TAD (Dixon et al., 2016).

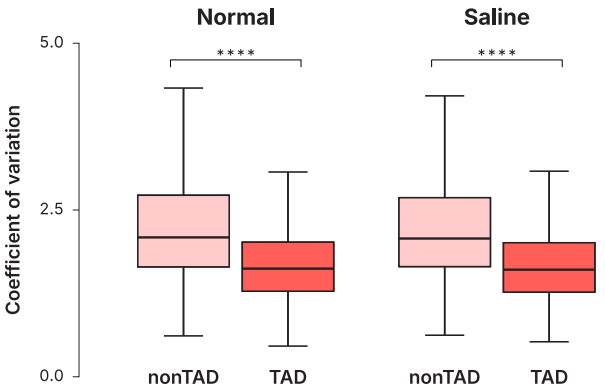

Figure 4. Gene co-expression in TAD domains.
The coefficient of variation (CV) of gene expression in TAD and non-TAD regions is measured using plants in normal and saline conditions in the greenhouse. Three biological replicates were used for each condition. Significance of two-tailed *t*-test is depicted by ns, non-significant; ****$P < 0.0001$.

Higher expression correlation between human and mouse orthologs was observed for genes within TADs compared with non-TAD genes (Krefting et al., 2018), and co-expressed gene pairs are significantly enriched within TADs in 12 vertebrate species (Li et al., 2022). This co-expression occurs because TADs restrict chromatin interactions between genes and distal regulatory elements. There is conflicting evidence, however, of such gene expression correlation in plants. Nützmann et al. (2020) found that genes within four biosynthetic gene clusters in Arabidopsis, maize, tomato, and rice were co-expressed, although this study did not include a genome-wide analysis. Indirect evidence for possible plant gene co-expression also comes from a poplar study, where pairs of paralogs located in conserved TADs showed more similar expression levels (Zhang, Zhao, et al., 2021). Only one genome-wide study, however – in maize – has investigated the relationship between gene expression and co-localization within TADs and concluded that genes within TADs were not co-expressed (Dong, Tu, Li, et al., 2020).

We tested whether TADs within rice are significantly co-expressed, using expression data from plants grown in the greenhouse under control and salinity stress conditions. We focused on identified TAD and non-TAD domains (remaining segments of the genome not identified as a TAD) (Figure S2a; Table S3). We found that genes within TAD domains show significantly lower levels of variation in expression compared to non-TAD regions (Figure 4). In normal greenhouse conditions, the mean coefficient of variation (CV) of gene expression in TADs is 1.69, while in non-TAD regions it is 2.49; in saline conditions, the mean CV for TADs = 1.68 and non-TAD regions = 2.46 (two-tailed *t*-test $P < 0.0001$). This result was also replicated under stress conditions in the greenhouse and field across multiple timepoints, as well as for TAD and non-TAD regions located within euchromatin and heterochromatin (Figures S4 and S5). To gain further support for our finding, we leveraged the publicly available Azucena root gene expression data measured under normal and aluminum stress conditions (Arbelaez et al., 2017), and were able to replicate our result (Figure S6). The lower variance of gene expression within TADs is consistent with the role of TADs in restricting the activity of regulatory elements (Harmston et al., 2017; Ibn-Salem et al., 2017), indicating that these inferred rice TADs may indeed represent functional units of gene co-expression.

TAD boundary strength is associated with distinct genetic and epigenetic features

TAD boundaries may exhibit varying levels of insulation as reflected in their insulation scores. Lower insulation scores indicate reduced contact frequencies between upstream and downstream loci and reflect a strong TAD boundary; these tend to be more conserved during evolution and harbor highly expressed genes, as shown in the recent comparative analysis of TADs in four different primates and four rodents which indicated that ultraconserved TADs have higher insulation strength (Okhovat et al., 2023). Similarly, stronger TAD boundaries have genes with higher expression than weak boundaries in the fungal plant pathogen *Verticillum dahlia* (Torres et al., 2024).

We classified boundaries based on their insulation scores and examined the relative enrichment of genetic and epigenetic marks at boundaries with low ('strong' boundaries) and high insulation scores ('weak' boundaries). We defined low and high insulation scores as ones falling into the lower and upper quartiles of the score distribution, respectively. We found that stronger boundaries have significantly higher levels of transcription (measured by PRO-Seq signals), although the difference is modest. They are also strongly associated with lower DNA methylation and active promoter-associated chromatin marks H3K27ac and H3K4me3. Interestingly, they are also depleted for H3K18ac, a histone mark associated with enhancers in *Drosophila*, that we showed is overall depleted at rice TAD boundaries. In summary, the strength of rice TAD boundaries was found to be associated with active epigenetic marks and negatively correlated with repressive chromatin. Our observations are corroborated by a recent analysis of Arabidopsis Micro-C data, which showed that the active histone mark H3K4me3 is a positive while repressive mark H3K27me3 is a negative predictor of boundary strength (Sun et al., 2024), suggesting these features may be generalizable across flowering plants.

In addition, we obtained PhastCons and fitCons (*r*) scores for the rice genome (Joly-Lopez et al., 2020), which are evolution-based measures of potential genomic function. PhastCons scores represent tribe-level interspecies

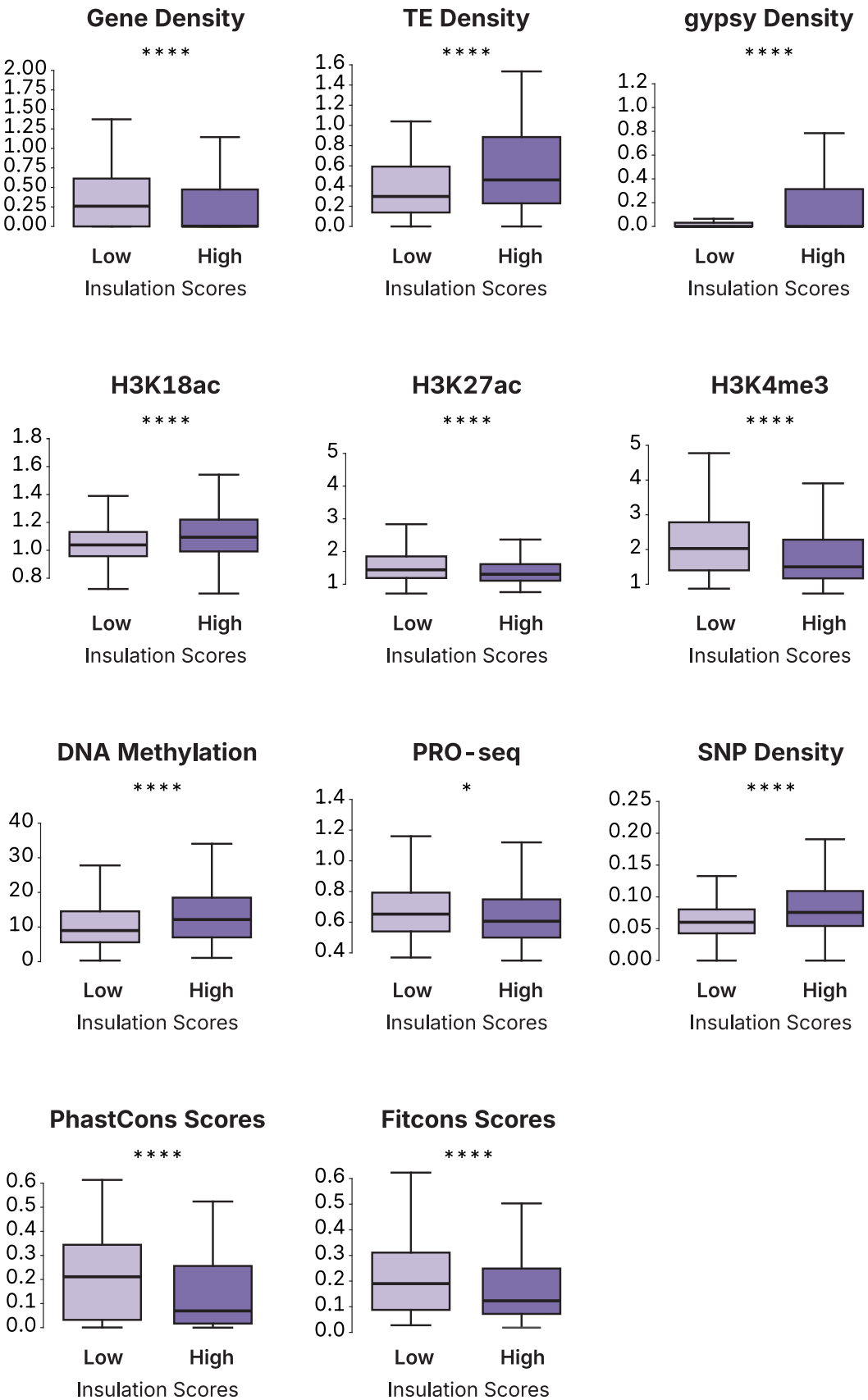

Figure 5. TAD boundary strength is associated with distinct genetic and epigenetic features.
Box plots show comparison of genetic and epigenetic features for strong (low insulation scores) and weak (high insulation scores) boundaries. *X*-axis represent average enrichment per 500 bp. Nipponbare TAD boundaries identified at 5 kb resolution. Significance of Wilcoxon rank-sum test depicted by ns, non-significant; $*P < 0.05$, and $****P < 0.0001$.

sequence conservation estimates, and fitCons scores provide probabilities that mutations at individual nucleotide sites have fitness consequences (Joly-Lopez et al., 2020). We find that stronger boundaries also have higher fitness consequences and PhastCons scores, suggesting purifying selection on these genomic regions. They also had higher gene density, lower SNP density, and lower TE content (Figure 5). Comparisons of boundaries with random genomic controls showed that weak boundaries share some characteristics with random regions (Figure S7). Interestingly, we found that stronger boundaries are specifically depleted of *gypsy* retrotransposons (Figure 5).

Global chromatin structure conservation correlates with evolutionary divergence time between genomes

In order to quantitatively compare the global 3D structure of different rice genomes, we utilized comparison of Hi-C Experiments using Structural Similarity (CHESS), a computer vision-based algorithm for the comparison of chromatin contact maps (Galan et al., 2020). CHESS provides a quantitative measure for similarity between a pair of normalized chromatin contact matrices, SSIM, with a value of 1 indicating identity between matrices, while 0 indicates no similarity. CHESS has previously been used to compare global chromatin conformation and extract differential features from *Drosophila melanogaster* wild type and mutant lines (Ing-Simmons et al., 2021) or *Fusarium graminearum* genomes under different conditions (Shao et al., 2024), and determine levels of chromatin conformation conservation between human and mouse (Galan et al., 2020), different species of fungal pathogens (Xia et al., 2022), and homologous blocks between X and Y chromosomes in primates (Zhou et al., 2023).

We started by ensuring that the various *Oryza* genomes were sufficiently colinear by aligning individual chromosomes (Marçais et al., 2018) and visualizing alignments as dotplots (Figure S7). We observed good colinearity between all genome pairs and detected a small number of large SVs more than 500 kb in size (Table S4). Of note, we detected a prominent large inversion on chromosome 6 that has previously been reported in *indica* genotypes (Kou et al., 2020). We masked large SVs and did a 500 kb sliding window analysis comparing Micro-C submatrices binned at 25 kb resolution across the genome between pairs of genomes; we generated similarity score (SSIM) and signal-to-noise (SN) ratios using CHESS for each pair of colinear genomic windows (Figure 6a; Figure S7).

We found that colinear genome regions share overall structural similarity between species/subspecies, but the degree of similarity differed between comparisons. To quantify overall similarity between genomes, we calculated the mode of the kernel density estimate (KDE) plot of similarity scores for colinear regions and corrected for random similarity by subtracting the modal value of SSIM for random regions, obtaining genome-wide normalized SSIM values (GN-SSIM). GN-SSIM values were highest for comparisons between biological replicates and lowest for the interspecies comparisons (Table S5).

Whether 3D genome conservation levels correlate with evolutionary distances between species remains largely unknown. Two *Drosophila* species separated by ~15 million years of divergence were found to share only 25% of TADs (Torosin et al., 2020), while in another study, two *Drosophila* species separated by ~49 million years were found to share 30–40% of TADs (Liao et al., 2021). In our study, we examine chromosome conformation divergence between more closely related species/subspecies; the genotypes analyzed have diverged between ~4000 and 5000 years ago (temperate versus tropical *japonica*) (Gutaker et al., 2020) to ~2.4 million years (between *O. sativa* and *O. meridionalis*) (Stein et al., 2018). To compare structural versus nucleotide sequence similarity between our *Oryza* genomes, we calculated pairwise synonymous substitution levels (dS) between coding sequences and found a significantly negative correlation between SSIM and dS ($P < 0.0371$) (Figure 6b,c). A neighbor-joining tree using the GN-SSIM values recapitulates the topology of the evolutionary tree of the *Oryza* species generated using sequence data (Figure S9) (Stein et al., 2018). Overall, the degree of global structural similarity was correlated with the degree of sequence similarity between genomes, and this result is in contrast with previous studies. For example, 3D genome conservation was assessed in distantly related *Anopheles* species, and the level of conservation was found to be similar for all pairwise species comparisons and did not correlate with evolutionary distance (Shao et al., 2024). In another study, chromatin conformation conservation was found to be independent of sequence conservation in fungi (Xia et al., 2022). Our results may indicate distinct principles of chromatin conformation evolution in plant genomes.

Genomic blocks with different structural similarity levels have distinct genetic and epigenetic properties

Our CHESS comparisons show that different genomic windows have different degrees of structural similarity (Figure 6a), indicating that they may be subject to different evolutionary constraints. This is especially evident in the

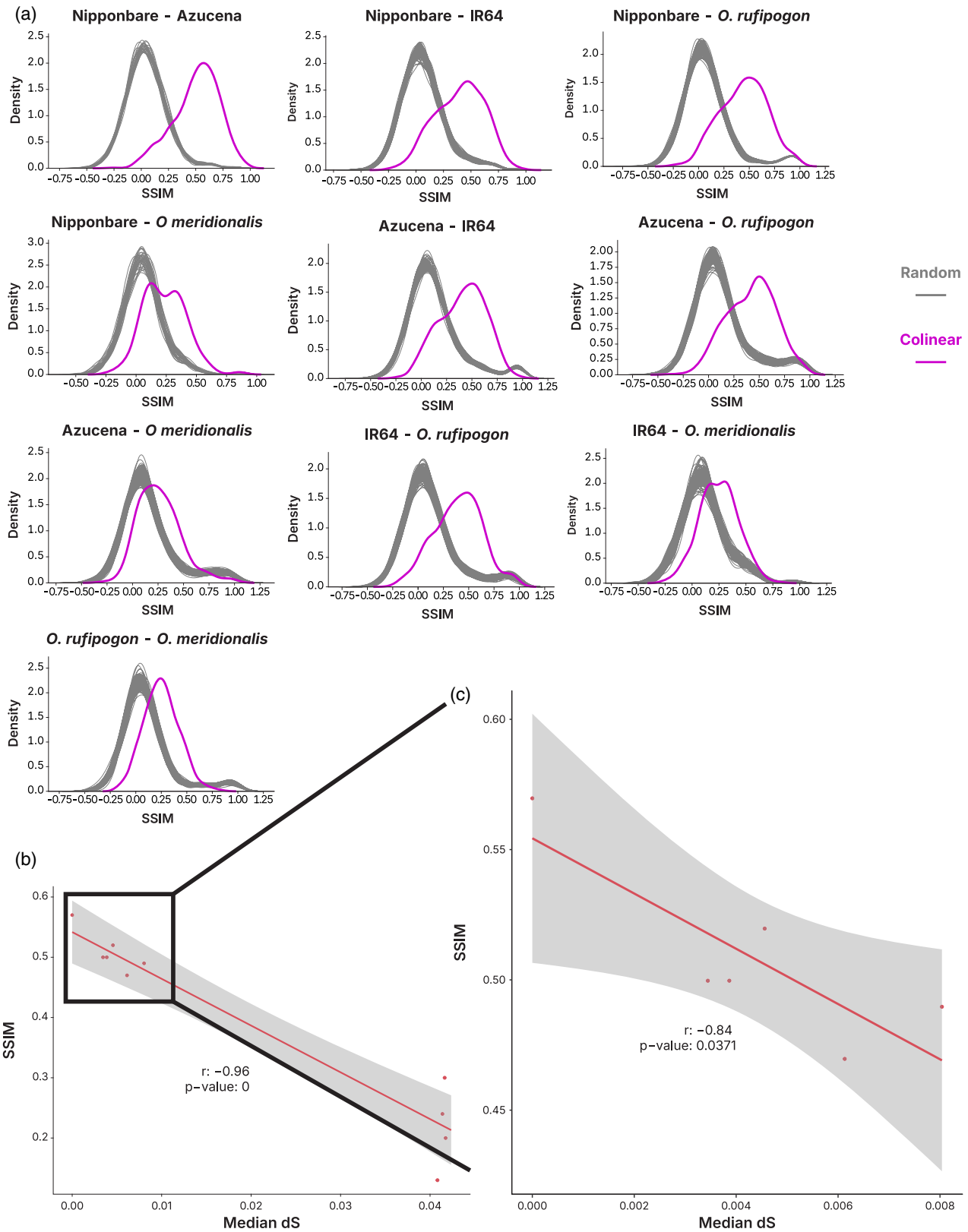

Figure 6. Global chromatin structure conservation correlates with evolutionary diversification time between genomes.
(a) Distributions of empirically determined CHESS scores for pairs of colinear (magenta) regions and 100 random permutations of region pairs (gray) for interspecies/subspecies comparisons.
(b) Three-dimensional sequence similarity correlates with 1D sequence divergence estimates. dS values were calculated from whole genome coding sequences. 95% regression confidence intervals are indicated.
(c) Same as (b), but with *O. meridionalis* excluded from pairwise comparisons.

O. sativa ssp. *japonica* (Nipponbare)/*O.meridionalis* comparison results, where we observed a bimodal distribution of SSIM scores (Figure 7a). To examine the nature of the genomic regions in these two modes of 3D chromosome similarity, we focused on 500 kb windows corresponding to each mode and analyzed the distribution of genetic and epigenetic features between these genomic regions.

We found that structurally similar genomic regions have higher sequence similarity, lower DNA methylation, higher gene density, higher H3K27ac and H3K4me3 content, and lower H3K27me3 content (Figure 7b). We also observe that these high-similarity genomic regions have higher FitCons and PhastCons scores, lower SNP density, and lower TE content (specifically *gypsy*, *copia* and SINE elements) (Figure S10). We then performed a similar analysis on genomic windows from the lower and upper tails of the SSIM distribution (Figure 7c) and found that 3D-similar regions have higher sequence similarity and lower DNA methylation levels (Figure 7d). We found a similar pattern when we analyzed the lower and upper tails of the *O. sativa* ssp. *japonica* (Nipponbare)/*O. rufipogon* SSIM distributions (Figure 7e,f). Taken together, our results show that genomic regions with conserved 3D structure across species are characterized by higher DNA sequence similarity, enriched in active gene-rich chromatin, and depleted for repressive marks.

Conserved TADs are gene-rich, actively transcribed regions

Our evolutionary analysis thus far focused on global 3D genome comparisons. We decided to look specifically at individual TADs and investigate their evolution within the five genomes. We employed two approaches: a widely used liftover-based (Dixon et al., 2012; Li et al., 2022; Torosin et al., 2020, 2022) and a BLAST-based approach (see "Methods" section) (Figures S11 and S12). In the first approach, we identified sets of high-confidence TADs, which resulted in the identification of TADs for Azucena (1187 TADs), Nipponbare (1425 TADs), IR64 (1352 TADs), *O. rufipogon* (1112 TADs) and *O. meridionalis* (1072 TADs) at 5 kb resolution. We considered TADs to be syntenic if the coordinates of the TADs in the other genomes reciprocally overlapped at least 50% with the Nipponbare TAD; this part of the analysis used Nipponbare as the anchor reference genome given its high level of annotation. After performing pairwise comparisons, we assigned each TAD to five conservation groups based on how many genomes the TAD was found in. 'Unique' represents Nipponbare-specific TADs, 'Rare' encompasses TADs found in two genomes, 'Moderately Conserved' – in three genomes, 'Highly Conserved' – in four genomes, and 'Core' – TADs found in all five genomes (Table S6). We analyzed TAD size, number of genes per TAD, mean gene expression, GC content, SNP/SV density, but found no significant differences between conservation groups. However, conserved TADs have significantly higher gene density and lower TE content (Figure S11b).

We complemented this analysis by implementing a BLAST-based approach (Figure S12). Briefly, we aligned Nipponbare TAD sequences to a database of Azucena TAD sequences, recording all hits per TAD and the total coverage per Nipponbare TAD. If the total coverage of the orthologous TAD was ≥50% of the reference TAD, it was recorded as conserved. We performed this for four pairs of genomes, using Nipponbare as the reference, and assigned Nipponbare TADs to five conservation groups following the logic previously described (Figure 8a; Table S6).

Using this approach, we found that more conserved TADs have higher gene content, lower TE content, and are enriched for the active chromatin mark H3K4me3 (Figure 8b). In agreement with the elevated gene content, conserved TADs also exhibit higher sequence conservation scores (Figure 8b; Figure S12). Conserved TADs have been found to be enriched for genes and active chromatin marks in *Drosophila* (Renschler et al., 2019) and legumes (Junaid et al., 2023). These and our findings highlight the general nature of 3D genome organization and TAD functionality across taxa. We also conducted a GO term analysis on genes within highly conserved and core TADs. Our results revealed an enrichment of biological processes related to fundamental cellular functions ('housekeeping'), which may explain the evolutionary conservation of these TADs.

Of note, in *O. sativa* inter-subspecies comparisons, only 38.9% of TADs were found to be conserved between Nipponbare and Azucena genomes, and 38.1% of TADs were conserved between Nipponbare and IR64. Thus, rice 3D genome organization shows low levels of intraspecific TAD conservation, similar to the 36% reported for two maize inbred lines (Tian et al., 2021); this suggests that

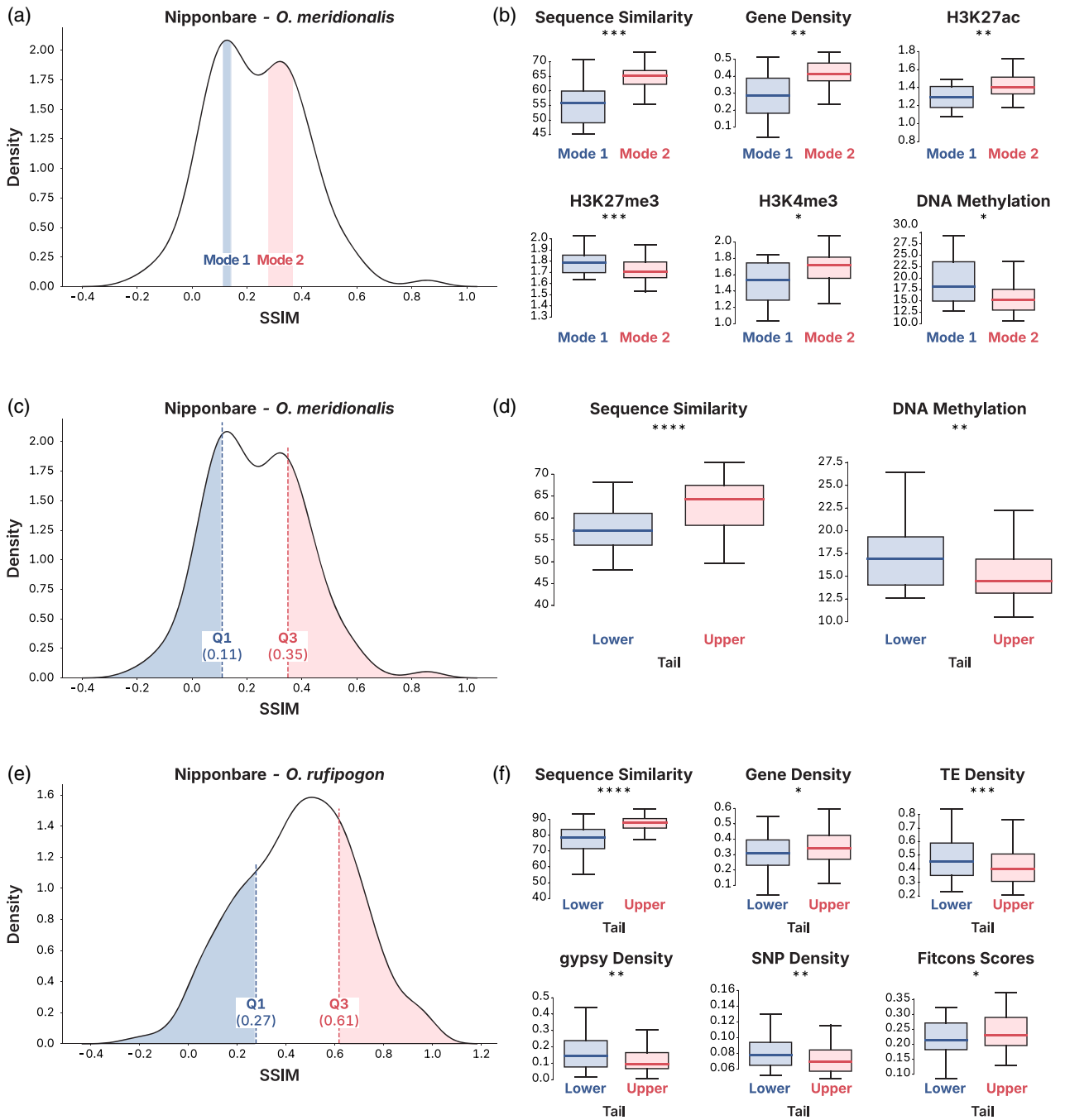

Figure 7. Genomic blocks with different structural similarity levels have distinct genetic and epigenetic properties.
(a) Distribution of empirically determined CHESS scores for the Nipponbare–*O. meridionalis* comparison with the regions around each mode highlighted.
(c) Distribution of empirically determined CHESS scores for the Nipponbare–*O. meridionalis* comparison with the upper and lower tails of the distribution highlighted. The first and third quartile values are indicated.
(e) Distribution of empirically determined CHESS scores for the Nipponbare–*O. rufipogon* comparison with the tails of the distribution highlighted. The first and third quartile values are indicated.
(b, d, f) Comparison of genetic and epigenetic features for genomic windows corresponding to the highlighted areas on the distribution plots. *X*-axis represent percentage of sequence similarity or average enrichment per 500 bp. Significance of Wilcoxon rank-sum test depicted by $*P < 0.05$, $**P < 0.01$, $***P < 0.001$, and $****P < 0.0001$.

plant TADs may be dynamic, fast-evolving structures. We note that some conserved TADs that have contracted/expanded in size have their boundaries coincident with structural variants (Figure 8c), implicating the role of SVs in rice TAD reorganization and possibly generating new gene expression patterns.

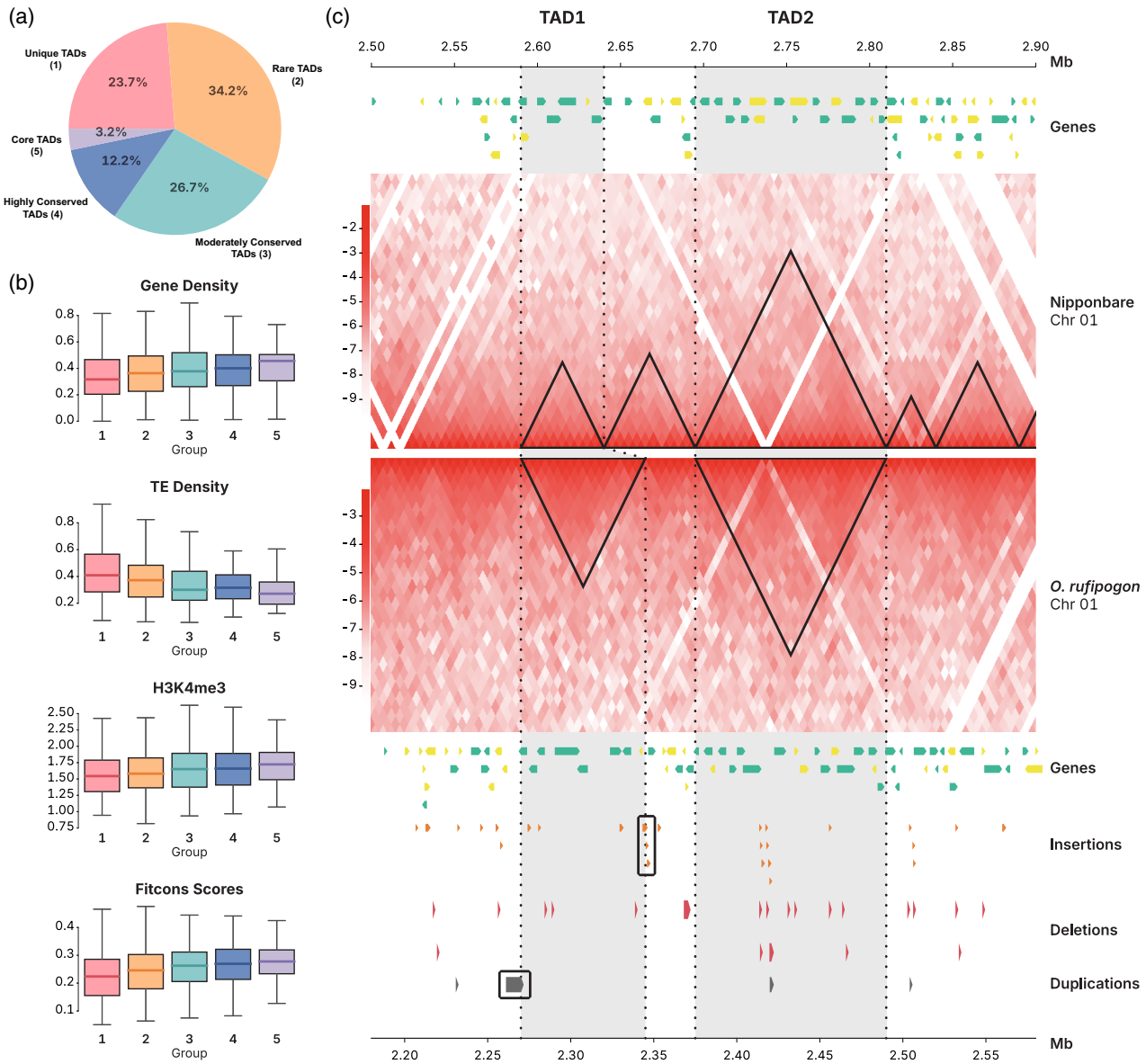

Figure 8. Rice TAD conservation.
(a) Nipponbare TADs assignment to five conservation groups using a BLAST-based approach.
(b) Comparison of gene and transposable element (TE) density, H3K4me3 mark, and fitcons scores for TAD conservation groups. *X*-axis represent average enrichment per 500 bp. The Wilcoxon rank-sum tests were performed for all pairwise comparisons between groups. Compact letters represent groups whose distributions of features were not significantly different from each other.
(c) Structural variants affect boundary rearrangements between *O. sativa* and *O. rufipogon*. Contact matrices with TADs (triangles) were plotted over a 400 kb section of chromosome 1 of *O. sativa* Nipponbare variety (top) and *O. rufipogon* (bottom). Conserved TADs are connected. Orthologous genes are in green, non-orthologous genes are in yellow. Matrix resolution is 5 kb.

Boundaries of conserved TADs are actively transcribed sequences enriched for sequence conservation signatures

Previous studies in vertebrates revealed that genetic and epigenetic properties of TAD boundaries vary depending on their level of sequence conservation. Conserved boundaries were found to have stronger insulation strength, enrichment of older TEs and higher gene densities (Li et al., 2022; Okhovat et al., 2023). There is some indication of similar behavior of plant TAD boundaries; for example, cultivar-specific TAD boundaries in cotton harbor more TEs than conserved boundaries (Long et al., 2021; Wang et al., 2021). To investigate whether similar trends can be observed for rice, we grouped TAD boundaries identified in Nipponbare based on whether they are conserved in other species/subspecies – a 'conserved' group where boundaries of TADs shared between at least four of our

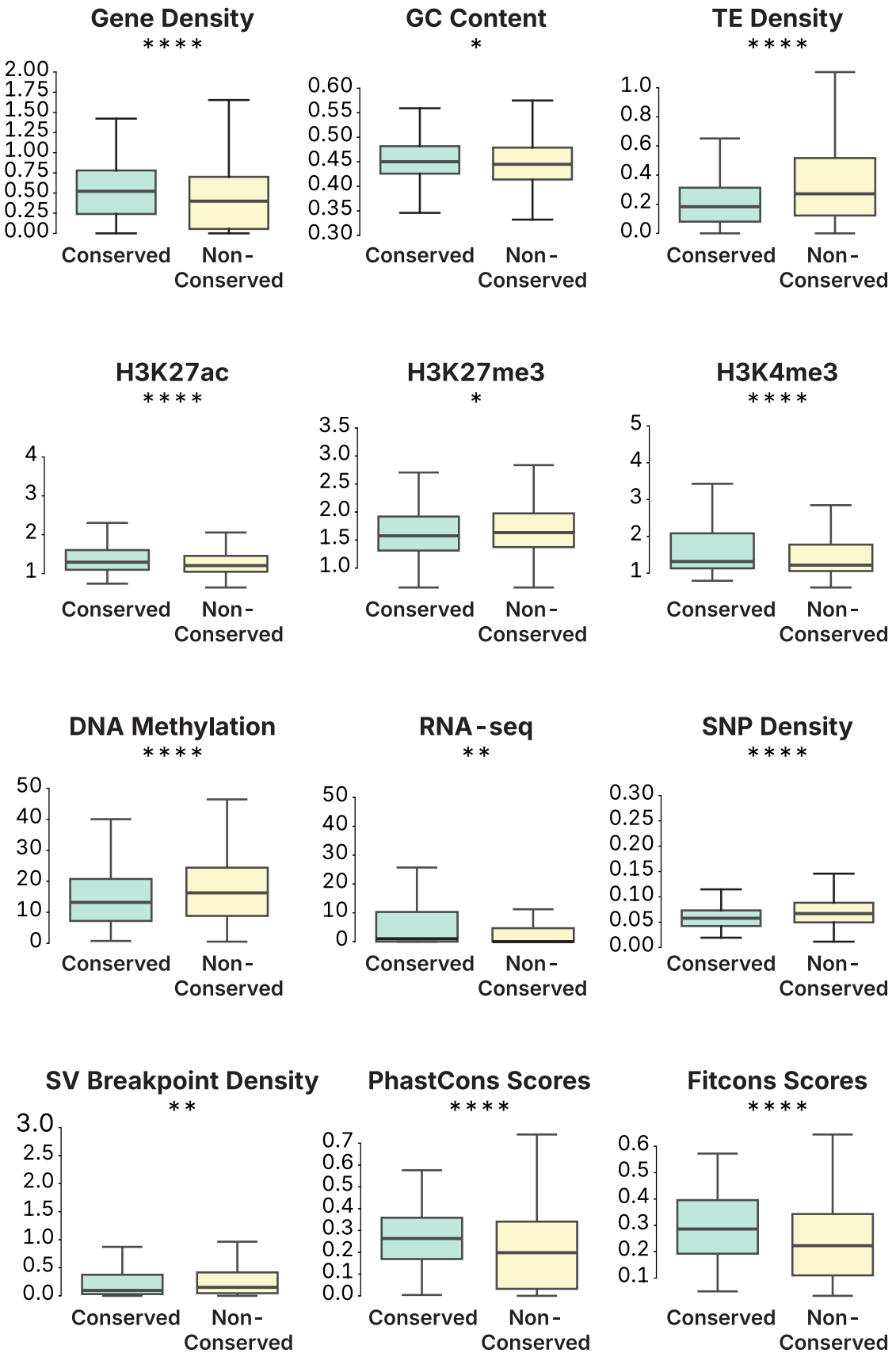

Figure 9. Boundaries of conserved TADs are actively transcribed sequences enriched for sequence conservation signatures.
Box plots show comparison of genetic and epigenetic features for conserved (yellow) and non-conserved (blue). *X*-axis represent average enrichment per 500 bp. Nipponbare TAD boundaries identified at 5 kb resolution. Significance of Wilcoxon rank-sum test depicted by ns, non-significant; $*P < 0.05$, $**P < 0.01$, and $****P < 0.0001$.

study genomes, and a 'non-conserved' group that are Nipponbare-specific.

We found that conserved boundaries had lower DNA methylation levels and H3K27me3 levels, but higher levels of active histone marks H3K27ac and H3K4me3. They also had higher gene content, lower TE content (specifically, DNA transposons and *gypsy* elements), higher GC content, and higher gene expression levels as measured by RNA-Seq (Groen et al., 2020), indicating that conserved TAD boundaries are transcriptionally active gene-dense regions (Figure 9; Figure S14). We also found that conserved TAD boundaries have higher FitCons and PhastCons values and are characterized by low SNP and SV breakpoint density (Figure 9), suggesting the action of purifying selection. Overall, boundaries conserved within rice genomes are gene-rich, active transcription regions with low DNA sequence variation, similar to what has been observed in cotton (Pei et al., 2022), human and mouse boundaries (Okhovat et al., 2023).

The nature of rice TADs and their evolution

The nature of three-dimensional genome structure has been of increasing interest in recent years, as higher order structures of the genome associated with functional features have been defined (Dekker & Heard, 2015; Dixon et al., 2012, 2016). A key 3D feature of genomes is TADs, which function as discrete genomic units and may serve as regulatory domains that facilitate co-regulated gene expression, at least in mammals (Dekker & Heard, 2015; Nora et al., 2012; Zhan et al., 2017) and *Drosophila* (Ramírez et al., 2018).

The nature of plant TADs, however, is less well understood, and indeed their functional significance in plants has been disputed (Dong, Tu, Li, et al., 2020; Nützmann et al., 2020; Zhang, Zhao, et al., 2021). Our analysis of TADs and their boundaries in rice provides evidence that these genomic elements share features with functional TADs in metazoan systems, including high transcriptional activity, enrichment for active histone marks, low methylation levels, low TE content, and increased gene densities at TAD boundaries. Moreover, we find significant correlation of expression levels for genes within these rice TADs, suggesting that they indeed function as genomic domains with shared regulatory features. Our findings emphasize that animal and plant TADs may share more commonalities than initially thought, as evidenced by similar genetic and epigenetic signatures associated with TADs and their boundaries.

Conservation of 3D genome topology is a highly contested topic in the field of comparative genomics (Eres & Gilad, 2021), and different computational approaches for TAD calling and arbitrary definitions of conservation status have resulted in a lack of consensus on whether the 3D genome is conserved between species. Nevertheless, a prevailing view within comparative 3D genomics is that TADs are highly conserved across species, although this has been challenged and has led to skepticism about the functional and evolutionary importance of TADs (Eres & Gilad, 2021). To address this problem, we quantitatively assessed global 3D genome topology conservation and diversity, as well as specific dissection of TADs and TAD boundaries. We showed that, on a global scale, chromosome topology between *Oryza* genomes that have diverged between ~4000 and 2.4 million years ago is largely conserved, and that 3D structural divergence is observed that correlates with evolutionary distance between genomes. However, we also show that individual TADs display low levels of conservation, even between subspecies, supporting previous findings made in other plant species such as foxtail millet, sorghum, legumes, and Arabidopsis (Dong et al., 2017; Junaid et al., 2023; Wang et al., 2021). We also demonstrate that different TAD groups have different levels of conservation, with conserved TADs being gene-dense, enriched for active chromatin marks, and depleted for TEs. We should note that we restricted evolutionary analysis to high-confidence TADs, identified with two callers independently, to ensure that the comparisons are based on the most reliable data. This approach helps ensure that observed differences reflect true evolutionary changes rather than artifacts of data noise or algorithmic variability.

How to explain this apparent discrepancy between TADs being functional units and yet generally not conserved between closely related species? One explanation may stem from the phenomenon of conserved functional neighborhoods with changing genes (Al-Shahrour et al., 2010). It was shown that the chromosomes of higher eukaryotes, including plants, contain genes arranged in functional neighborhoods with gene co-expression, similar to genes arranged into clusters within a TAD (Al-Shahrour et al., 2010). The function of a cluster is constrained within a neighborhood, and if a chromosomal rearrangement breaks a neighborhood, selective pressure will lead to the formation of another neighborhood with similar function through additional chromosomal rearrangements (Al-Shahrour et al., 2010). Similar mechanisms could explain

the seeming instability of TADs in evolution. In addition, high levels of presence/absence variation known for plant genomes, including rice, could also contribute to the highly dynamic nature of the TAD genomic landscape. Future studies can indeed examine the evolutionary mechanisms underlying the divergence of TADs in eukaryotic genomes and their functional consequences.

METHODS

Plant materials and growth conditions for Micro-C

Seeds of *O. sativa* landraces Nipponbare (IRGC 12731, temperate japonica), Azucena (IRGC 328, tropical japonica), and IR64 (IRGC 66970, indica) were provided by the International Rice Research Institute (Los Baños, Philippines). Seeds of *O. rufipogon* (W1943) and *O. meridionalis* (W2112) were provided by the National Institute of Genetics (Mishima, Japan). Seeds were incubated for 5 days at 50°C and germinated in water in the dark for 48 h at 30°C. These were subsequently sown on hydroponic pots suspended in 1 × Peters solution and 1.8 mM $FeSO_4$ (pH = 5.1–5.8) (JR Peters). Plants were grown in growth chambers (12 hour light/12 hour dark cycle; 30°C/20°C day/night; 300–500 μmol quanta m^{-2} sec^{-1}; relative humidity: 50–70%). Leaf tissue was collected from 14-day-old plants.

Micro-C library preparation and sequencing

For each species/variety, we generated two replicate Micro-C datasets (Table S1). The Micro-C libraries were prepared using the Dovetail Micro-C Kit (Dovetail Genomics, Scotts Valley, CA, USA) for animal tissue, which we adapted for plant tissues. In brief, 50 mg of frozen leaf tissue were ground to a fine powder in liquid nitrogen. Ground tissue was fixed with disuccinimidyl glutarate and formaldehyde. The cross-linked chromatin was then digested using micrococcal nuclease (MNase) until an optimal digestion profile of 40–70% mononucleosomes was achieved. The sample was then lysed with SDS, and the chromatin ends were repaired and ligated to a biotinylated bridge adapter followed by proximity ligation. The cross-links were then reversed, the proteins were degraded, and the DNA was purified and ligated with Illumina-compatible adaptors. Biotinylated DNA was pulled down on streptavidin beads and then PCR amplified. Two biological replicates were used. The libraries were sequenced on the Illumina NextSeq 500 platform (Illumina, San Diego, CA, USA) with 150-bp paired-end reads at the NYU CGSB Genomics Core facility.

Micro-C data analysis

Chromatin contact maps were generated using the Dovetail Genomics pipeline (https://micro-c.readthedocs.io/en/latest/index.html). Briefly, sequenced read pairs were mapped to the reference genomes (see below) using BWA-MEM v.0.7.17 (Li & Durbin, 2009), then low-quality reads (MAPQ < 40) and PCR duplicates were removed by pairtools v.1.0.2 (Open2C et al., 2023). Hic and mcool files (that included multiple bin sizes) were generated by juicer v.1.6 (Durand, Shamim, et al., 2016) and cooler v.0.9.0 (Abdennur & Mirny, 2020), respectively. Hic files were normalized by the KR method in Juicebox v.2.20.00 (Durand, Robinson, et al., 2016), and cooler balance was applied to normalize mcool files. CoolBox v.0.3.8 (Xu et al., 2021) was used for plotting the contact maps at 5 kb resolution together with genetic/epigenetic tracks and for plotting the distance-dependent decay of chromatin contacts. We used HiCRep (Yang et al., 2017) to calculate the stratum-adjusted correlation coefficient (SCC) at 5 kb resolution with the following parameters: h = 30, lbr = 0, ubr = 1 000 000. We calculated SCC values between biological replicates for each chromosome of each species, then averaged the values for all chromosomes. The average SCC values ranged from 0.76 to 0.88. HiCRes (Marchal et al., 2022) was used to estimate the maximum contact map resolution.

Compartment calling

We called A/B compartments by implementing the fanc compartments tool from the FAN-C package (Kruse et al., 2020). The fanc compartments command produces a correlation matrix from a contact matrix file binned at 160 kb resolution. Compartment matrices are calculated on a per-chromosome basis. Then, the eigenvector of the correlation matrix was used to make compartment calls. The average GC content of regions with positive and those with negative eigenvector entries was used to determine the compartment type of genomic regions. As GC content has previously been shown to correlate well with compartmentalization, the eigenvector was oriented such that negative entries correspond to B (low GC content) and positive entries to A (high GC content) compartments. TAD and non-TAD regions were assigned to A/B compartments if more than 50% of the region fell within the respective compartment.

TAD annotation

We compared the performance of three tools for TAD identification: hicFindTADs from the HiCExplorer v.3.7.2 package (Ramírez et al., 2018), HiTAD from TADLib (Wang et al., 2017), and Arrowhead from the juicer package (Durand, Shamim, et al., 2016). We called TADs in the Azucena genome at three resolutions: 1, 2, and 5 kb. HiTAD detects hierarchical TADs, including TADs, sub-TADs, and smaller domains. For our analysis, we used only TADs level 0. The number of TADs called by each tool can be found in Table S2, and we noted that they were similar for HiCExplorer and HiTAD. We then generated metagene plots for the repressive (DNA methylation, H3K27me3) and active (H3K4me3, H3K27ac) marks using deepTools v.3.5.2 (Ramírez et al., 2016). We expected TAD boundaries to be enriched for active chromatin marks and depleted for repressive marks. Based on the distribution of signal (Figure S15), we concluded that TADs were most accurately called by HiCExplorer at 1, 2, and 5 kb resolutions, and by HiTAD at 2 and 5 kb resolutions. We then identified a uniform set of TADs called by both HiCExplorer and HiTAD tools at 2 and 5 kb resolutions, with the criteria that the TAD body must reciprocally overlap by at least 80% between both tools. The TAD body and boundaries identified by HiCExplorer were retained as the consensus. TAD boundaries were defined as 2 and 5 kb genome fragments identified by hicFindTADs from HiCExplorer. The same approach for calling TADs and TAD boundaries was applied to the remaining *Oryza* genomes, except that only the 5 kb resolution was considered.

Genetic and epigenetic features of TADs and boundaries

We used *pybedtools* v.0.9.1, a Python wrapper for BEDTools (Dale et al., 2011) to analyze the enrichment of genetic and epigenetic features between TADs/non-TADs/TAD boundaries and TAD conservation groups. We performed Wilcoxon rank sum tests for all pairwise comparisons between the groups and corrected the resulting *p* values using the Benjamini–Hochberg procedure. Metagene plots of the distribution of features across TADs were generated with deepTools (Ramírez et al., 2016).

Repeat masking of genomes

We performed two rounds of repeat masking of the five genomes used with RepeatMasker v.4.1.2 (https://www.repeatmasker.org/), using default repeat libraries and the Oryza Repeat Database from the Rice Genome Annotation Project (http://rice.uga.edu), which resulted in about 43% of the genomes masked.

Identification of conserved TADs

We used two approaches to identify conserved TADs. For the liftOver-based approach, we first generated chain files for pairs of repeat-masked genomes using custom scripts based on the UCSC pipeline (http://genomewiki.ucsc.edu/index.php/LiftOver_Howto). We then lifted over the genomic coordinates of TADs from the query to the target (Nipponbare) genome with the UCSC liftOver tool (Hinrichs et al., 2006). To be successfully lifted over, TADs in one genome require a 20% minimum ratio of bases (-minMatch = 0.20) to be remapped in the other genome. Lifted-over TADs from the query genome that reciprocally overlapped a TAD in the target genome by at least 50% were identified with BEDTools (Quinlan & Hall, 2010) *intersect* (-r 0.5) and recorded as conserved. We performed this for four pairs of genomes and assigned Nipponbare TADs to five conservation groups.

For the BLAST-based approach, we first generated a database of TAD sequences with BEDTools *getfasta*. Then, the database of the query species was aligned to the target species database using BLASTn (blast+ v.2.13.0) (Camacho et al., 2009), and the results were filtered with custom Python code so that only TADs on the same chromosome in query and target remained, and all hits per TAD and the total coverage were recorded. If the total coverage of the target species' TAD was ≥50% of the query species' TAD, it was recorded as conserved. We performed this for four pairs of genomes and assigned Nipponbare TADs to five conservation groups.

Boundary motif enrichment

TAD boundaries identified at resolutions 2 and 5 kb were used to identify motifs enriched at boundaries. We used HOMER v.4.11 (Heinz et al., 2010) with two sets of parameters (*-len 10 -size given* and *-len 8,10,12 -size 200*). We also used STREME from the MEME Suite v.5.3.0 (Bailey, 2021) with default parameters. For background, randomly chosen non-boundary sequences were used. The motifs found to be significantly enriched by both tools in both sets of boundaries were reported.

GO enrichment

We analyzed whether genes at TAD boundaries are enriched for specific functional categories using the enrichGO function in clusterProfiler v.4.0 (Wu et al., 2021). We ran clusterProfiler for all three ontologies: biological process, molecular function, and cellular component.

TE annotation

The IRGSP rice6.9.5.liban TE library (Ou et al., 2019) was complemented with additional, high-confidence TE consensuses from the wild rice genome (*Oryza rufipogon*). In order to do this, EDTA was run on *O. rufipogon* GCA_000817225.1 assembly, retaining only TE consensuses without homology to the rice6.9.5.liban library. These novel sequences were further filtered to avoid false positives by retaining only those longer than 200 bp and carrying a conserved TE domain (as identified by TEsorter; Zhang et al., 2022) or containing more than three full-length copies in the genome (more than 90% of consensus length). The combined library was used to annotate IRGSP and Azucena genome assemblies using RepeatMasker v.4.1.2 (https://www.repeatmasker.org/).

RNA-Seq analysis

We grew three replicates of Azucena in Yoshida culture solution (based on Ahmadizadeh et al., 2016) in the Lloyd T. Evans Plant Growth Facility (PGF) of the International Rice Research Institute, Los Baños, Philippines greenhouse under normal (0 dS m^{-2} equivalent to 0 mM NaCl) and saline (10 dS m^{-2} equivalent to 100 mM NaCl solution) conditions. Tissue samples were collected from the third leaf at specific time points and immediately soaked in RNAlater™ Stabilization Solution (Invitrogen, Carlsbad, CA, USA). Total RNA was extracted using RNeasy Plant Mini Kits (Qiagen, Germantown, MD, USA; Cat No. 74904). Contaminating DNA was removed from the total RNA samples by treatment with RNase-free DNase (Qiagen, Germantown, MD, USA; Cat No. 79254). RNA quality was determined by gel electrophoresis. Strand-specific RNA-Seq libraries were synthesized using the NEBNext® Ultra™ II Directional RNA Library Prep kit (New England Biolabs, Ipswich, MA, USA). The libraries were sequenced at nine libraries per lane using standard methods for paired-end 51 base-pair reads on an Illumina HiSeq 2500 (Illumina, San Diego, CA, USA) at the NYU CGSB Genomics Core facility. Demultiplexed reads were aligned to transcripts from the *Oryza sativa* Japonica assembly IRGSP-1.0 (GCA_001433935.1) and counted with kallisto (v0.46.0) and then processed into a gene count matrix. The read counts obtained were normalized using the TMM (trimmed mean of *M* values) method with edgeR v4.2.1 (Robinson et al., 2010), and then averaged over the replicates for each timepoint per environment. Transcripts that were expressed (read count >0) in at least 8 of the 10 samples were chosen for downstream analyses, leading to a total of 34 716 expressed transcripts.

Co-expression analysis

We estimated the coefficient of variation, defined as the standard deviation (SD) by mean (CV = SD/mean), as a measure of gene co-expression. For this, we chose TAD and non-TAD domains with at least five genes expressed, giving us a total of 1247 domains (678 TAD domains and 569 non-TAD domains). Here, we focus on the results from normal conditions timepoint 1 (0 min) in the main manuscript and attach the results from all other timepoints and conditions in the Supplementary figures. Additionally, we estimated the CV for TAD and non-TAD domains using previously published leaf tissue drought and salinity stress data from the field (Groen et al., 2020; Gupta et al., 2025), and aluminum stress data for roots (Arbelaez et al., 2017).

Epigenetic marks

DNA methylation and histone marks ChIP-seq sample preparation, sequencing, and data analysis for *O. sativa* Azucena variety were performed as described in Joly-Lopez et al. (2020), except for the sequencing reads that were aligned to the Azucena genome assembly.

Genome alignments

The following reference genomes were used: *O. sativa* Nipponbare (IRGSP-1.0), *O. sativa* Azucena (PRJNA424001), *O. sativa* IR64 (PRJNA509165), *O. rufipogon* (PRJEB4137), and *O. meridionalis* (PRJNA48433). To make sure the genomes are colinear, we aligned the individual chromosomes pairwise using the nucmer

utility (with parameters --mum -l 100 -c 1000 -d 50) from the MUMmer4 software package v.4.0.0 (Marçais et al., 2018) and visualized the alignments as dotplots using the mummerplot post-script command (Figure S7). We observed good collinearity between all pairs of comparisons and detected a small number of large SVs (defined as more than 500 kb in size). To extract the coordinates of large SVs (Table S4), we first filtered the alignments with the delta-filter utility of MUMmer (-m -i 90 -l 100), then applied the show-coords utility and custom scripts.

Detection of structural variants

We used MUM&Co v3.8 (O'Donnell & Fischer, 2020) to detect insertions, deletions, and duplications in fragments of chromosomes between genomes. The three classes of SVs from output tsv files were converted into bed files using custom Python code and visualized in CoolBox (Xu et al., 2021).

Identification of colinear genomic blocks

To generate pairs of genomic windows for CHESS analysis, we first masked the identified large SVs from the genomes. We then split one of the genomes in the pair into 500 kb fragments with a step size of 250 kb. Next, we lifted over the coordinates of the start and end of the blocks using the UCSC *liftOVer* utility, generating bedpe files with pairs of colinear genomic blocks.

Comparison of colinear genomic blocks

We used CHESS v.0.3.8 (Galan et al., 2020) to compare global genome conformation between species/varieties. We compared Micro-C submatrices binned at 25 kb resolution across the genome between pairs of genomes to generate a similarity score (SSIM) and signal-to-noise (SN) ratio for each pair of colinear genomic windows. We then filtered out the genomic windows with SN <0.5 and plotted the distribution of SSIM for resulting windows together with the distributions of SSIM for 100 random permutations of region pairs. Using this approach, we compared all combinations of five genomes (10 comparisons). For control, we compared the Micro-C submatrices of biological replicates for each accession (Figure S8). To quantify the overall similarity between genomes, we calculated the mode of the KDE plot of the similarity scores for colinear regions and subtracted from that the mode of the KDE plot of SSIM for random regions, obtaining a genome-wide normalized SSIM value (GN-SSIM). All GN-SSIM values for the interspecies/varieties comparisons were significantly different from the biological replicates' GN-SSIM values (*t*-test).

We compared the enrichment for genetic and epigenetic features between groups of genomic windows with *pybedtools* (Dale et al., 2011). To calculate sequence similarity between pairs of windows, we first extracted the sequences of 500 kb windows in FASTA format using Biopython (https://github.com/biopython/biopython), aligned them pairwise with EMBOSS Stretcher (Madeira et al., 2022) and recorded the sequence identities using custom code. To control for possible biases introduced by the different mappability of the genomic windows, we calculated mappability scores using GenMap (with parameters -K 30 -E 2) (Pockrandt et al., 2020), which computes the uniqueness of k-mers for each position in the genome. We compared the mappability scores for the groups of genomic windows analyzed and found that they were not significantly different. To compare the level of structural similarity with the level of sequence similarity between genomes, we calculated synonymous substitution levels (dS) between coding sequences using the orthologr v.0.4.2 package (Drost et al., 2015).

DATA ANALYSIS TOOLS

HOMER v.4.11, STREME v.5.3.0, BWA-MEM v.0.7.17, pairtools v.1.0.2, GenMap, HicRes, HicRep, Orthologr v.0.4.2, DeepTools v.3.5.2, MUMmer4, MUM&Co v.3.8, CoolBox v.0.3.8, HiCExplorer v.3.7.2, HiTAD, Arrowhead, juicer v.1.6, Juicebox v.2.20.00, cooler v.0.9.0, Pybedtools v.0.9.1, BEDTools v.2.30.00, EMBOSS Stretcher, Biopython, blast+ v.2.13.0, UCSC liftOver, RepeatMasker v4.1.2, edgeR v.4.2.1, FAN-C v.0.9.1.

ACKNOWLEDGMENTS

We would like to thank members of the Purugganan laboratory for critical discussions throughout this work, and Ramin Rahni for graphic design support. The wild rice accessions used in this study were distributed from the National Institute of Genetics supported by the National Bioresource Project, MEXT, Japan. This work was funded in part by grants from the National Science Foundation, Zegar Family Foundation, and Tamkeen/NYU Abu Dhabi Research Institute to M.D.P.; European Social Fund Plus' to R.C.; Ministerio de Ciencia e Innovación and Severo Ochoa Center of Excellence in R&D to R.C. and J.M.C.

CONFLICT OF INTEREST

The authors declare no conflicts of interest.

DATA AVAILABILITY STATEMENT

The Micro-C and RNA-Seq data have been deposited to NCBI SRA under the accession numbers PRJNA1121389 and PRJNA1198503, respectively.

SUPPORTING INFORMATION

Additional Supporting Information may be found in the online version of this article.

Figure S1. Chromatin contact probabilities as a function of genomic distance.

Figure S2. Genome GC content by TAD features. (a) Partition of the genome into three classes of genomic regions. Triangles on top depict the extent of the TAD, while bidirectional arrows at the bottom show the different classes of TAD features. (b) TAD boundaries (TADbr) have the highest GC content followed by non-TAD bodies (non-TAD_{body}) and then TAD bodies (TAD_{body}). Significance of two-tailed *t*-test depicted by ns, non-significant; $*P < 0.05$, $**P < 0.01$, $***P < 0.001$, and $****P < 0.0001$.

Figure S3. Gene ontology enrichment analysis for genes at Azucena TAD boundaries identified at 5 kb resolution. BP, biological process; CC, cellular component; MF, molecular function.

Figure S4. Gene co-expression in TAD domains. Shown here is the coefficient of variation (CV) measured using plants in the normal (a) and saline (b) in the greenhouse at multiple timepoints (60, 180, 240, and 5 days), and in the field exposed to drought stress (c) and salinity stress (d). Significance of two-tailed *t*-test depicted by ns, non-significant; $*P < 0.05$, $**P < 0.01$, $***P < 0.001$, and $****P < 0.0001$.

Figure S5. Gene co-expression in TAD domains within A and B compartments. Shown here is the coefficient of variation (CV) measured using plants in the normal (a, c) and saline (b, d) in the greenhouse at multiple timepoints (60, 180, 240, and 5 days). TAD and non-TAD regions were assigned to A/B compartments if more

than 50% of the region falls within a respective compartment. Significance of two-tailed *t*-test depicted by ns, non-significant; $*P < 0.05$, $**P < 0.01$, $***P < 0.001$, and $****P < 0.0001$.

Figure S6. Gene co-expression in TAD domains in root tissue. Shown here is the coefficient of variation (CV) measured using plants in the normal and aluminum stress conditions. Significance of two-tailed *t*-test depicted by ns, non-significant; $*P < 0.05$, $**P < 0.01$, $***P < 0.001$, and $****P < 0.0001$.

Figure S7. Comparison of strong and weak TAD boundaries with random genomic regions. Box plots show comparison of genetic and epigenetic features for strong (low insulation scores) and weak (high insulation scores) boundaries, as well as random 5 kb genomic regions. Significance of Wilcoxon rank-sum test depicted by ns, non-significant; $*P < 0.05$, $**P < 0.01$, $***P < 0.001$, and $****P < 0.0001$.

Figure S8. Genome collinearity within *Oryza* visualized using MUMmer. The nucmer utility with parameters --mum -l 100 -c 1000 -d 50 was used to align individual chromosomes pairwise.

Figure S9. Distributions of empirically determined CHESS scores. Plots are for indicated pairs of colinear (magenta) regions and 100 random permutations of region pairs (gray) for comparisons of biological replicates.

Figure S10. Neighbor-joining tree constructed using the GN-SSIM values recapitulates the topology of the evolutionary tree of the *Oryza* species. (a) Calculation of GN-SSIM value from the distribution of empirically determined CHESS scores for pairs of colinear (magenta) regions and 100 random permutations of region pairs (gray). (b) Rate of global chromatin structure evolution. GN-SSIM values were used to create a distance matrix to construct the neighbor-joining tree. (c) Evolutionary tree of the *Oryza* species constructed using genome-wide median dS values. dS values were computed for all coding sequences with orthologr. Median dS values were calculated for all genomes pairwise and then used to create a distance matrix.

Figure S11. Comparison of genetic and epigenetic features for genomic windows corresponding to the two modes of the KDE plot of SSIM values for the Nipponbare–*O. meridionalis* comparison. Structurally similar genomic regions have higher fitcons and PhastCons scores, lower SNP density and lower TE content (specifically *gypsy*, *copia*, and SINE elements). Significance of Wilcoxon rank-sum test depicted by ns, non-significant; $*P < 0.05$, $**P < 0.01$, $***P < 0.001$, and $****P < 0.0001$.

Figure S12. Detecting conserved TADs using liftover-based approach. (a) Schematic representation of the liftover-based conserved TADs identification method. (b) Conserved TADs have higher gene coverage and lower TE content.

Figure S13. TAD conservation analysis with BLAST: detecting conserved TADs with SVs. (a) Schematic representation of the BLAST-based approach to identify conserved TADs. (b) Distribution of conserved TAD coverages per genome pair analyzed. (c) Distribution of conserved TAD coverages per genome pair analyzed, but only the coverages above 50% plotted.

Figure S14. Comparison of PhastCons scores for TAD conservation groups. Group 5 represents TADs with orthologs in all five genomes, Group 1 represents Nipponbare-specific TADs. The Wilcoxon rank-sum tests were performed for all pairwise comparisons between groups. Compact letters represent groups whose distributions of features were not significantly different from each other.

Figure S15. Conserved TAD boundaries have lower density of *gypsy* elements and DNA transposons. Shown here are comparisons of TE density for strong (low insulation scores, yellow) and weak (high insulation scores, blue) Nipponbare TAD boundaries identified at 5 kb resolution. Significance of Wilcoxon rank-sum test depicted by ns, non-significant; $*P < 0.05$, $**P < 0.01$, $***P < 0.001$, and $****P < 0.0001$.

Figure S16. The distribution of epigenomic features across TADs called with different tools at different resolutions. TADs were linearly transformed to align the panel's borders. Boundaries were marked as '0', and the plots span 20 kb proximal and distal to the boundaries.

Table S1. Micro-C libraries and contact map statistics.

Table S2. Number of TADs identified with different tools in Azucena.

Table S3. Properties of spatial chromatin features.

Table S4. Large (>500 kb) structural variants detected with mummer4.

Table S5. GN-SSIM scores.

Table S6. Number of TADs in conservation groups.

REFERENCES

Abdennur, N. & **Mirny, L.A.** (2020) Cooler: scalable storage for Hi-C data and other genomically labeled arrays. *Bioinformatics*, **36**(1), 311–316.

Ahmadizadeh, M., **Vispo, N.A.**, **Calapit-Palao, C.D.O.**, **Pangaan, I.D.**, **Viña, C.D.** & **Singh, R.K.** (2016) Reproductive stage salinity tolerance in rice: a complex trait to phenotype. *Indian Journal of Plant Physiology*, **21**(4), 528–536.

Al-Shahrour, F., **Minguez, P.**, **Marqués-Bonet, T.**, **Gazave, E.**, **Navarro, A.** & **Dopazo, J.** (2010) Selection upon genome architecture: conservation of functional neighborhoods with changing genes. *PLoS Computational Biology*, **6**(10), e1000953.

Arbelaez, J.D., **Maron, L.G.**, **Jobe, T.O.**, **Piñeros, M.A.**, **Famoso, A.N.**, **Rebelo, A.R.** ***et al.*** (2017) ALUMINUM RESISTANCE TRANSCRIPTION FACTOR 1 (ART1) contributes to natural variation in aluminum resistance in diverse genetic backgrounds of rice (*O. sativa*). *Plant Direct*, **1**(4), e00014.

Bailey, T.L. (2021) STREME: accurate and versatile sequence motif discovery. *Bioinformatics*, **37**(18), 2834–2840.

Bing, X., **Ke, W.**, **Fujioka, M.**, **Kurbidaeva, A.**, **Levitt, S.**, **Levine, M.** ***et al.*** (2024) Chromosome structure I: loop extrusion or boundary:boundary pairing? *eLife*, **13**, RP94070.

Bonchuk, A., **Maksimenko, O.**, **Kyrchanova, O.**, **Ivlieva, T.**, **Mogila, V.**, **Deshpande, G.** ***et al.*** (2015) Functional role of dimerization and CP190 interacting domains of CTCF protein in *Drosophila melanogaster*. *BMC Biology*, **13**(1), 1–23. Available from: https://doi.org/10.1186/s12915-015-0168-7

Bouwman, B.A.M. & **de Laat, W.** (2015) Getting the genome in shape: the formation of loops, domains and compartments. *Genome Biology*, **16**(1), 154. Available from: https://doi.org/10.1186/s13059-015-0730-1

Camacho, C., **Coulouris, G.**, **Avagyan, V.**, **Ma, N.**, **Papadopoulos, J.**, **Bealer, K.** ***et al.*** (2009) BLAST+: architecture and applications. *BMC Bioinformatics*, **10**(1), 421.

Dale, R.K., **Pedersen, B.S.** & **Quinlan, A.R.** (2011) Pybedtools: a flexible python library for manipulating genomic datasets and annotations. *Bioinformatics (Oxford, England)*, **27**(24), 3423–3424.

Dang, D., **Zhang, S.W.**, **Duan, R.** & **Zhang, S.** (2023) Defining the separation landscape of topological domains for decoding consensus domain organization of 3D genome. *Genome Research*, **33**(3), 386–400.

Dekker, J. & **Heard, E.** (2015) Structural and functional diversity of topologically associating domains. *FEBS Letters*, **589**(20), 2877–2884.

Dixon, J.R., **Gorkin, D.U.** & **Ren, B.** (2016) Chromatin domains: the unit of chromosome organization. *Molecular Cell*, **62**(5), 668–680.

Dixon, J.R., **Selvaraj, S.**, **Yue, F.**, **Kim, A.**, **Li, Y.**, **Shen, Y.** ***et al.*** (2012) Topological domains in mammalian genomes identified by analysis of chromatin interactions. *Nature*, **485**(7398), 376–380.

Doğan, E.S. & **Liu, C.** (2018) Three-dimensional chromatin packing and positioning of plant genomes. *Nature Plants*, **4**(8), 521–529. Available from: https://doi.org/10.1038/s41477-018-0199-5

Dong, F. & **Jiang, J.** (1998) Non-Rabl patterns of centromere and telomere distribution in the interphase nuclei of plant cells. *Chromosome Research*, **6**(7), 551–558.

Dong, P., **Tu, X.**, **Chu, P.Y.**, **Lü, P.**, **Zhu, N.**, **Grierson, D.** ***et al.*** (2017) 3D chromatin architecture of large plant genomes determined by local A/B compartments. *Molecular Plant*, **10**(12), 1497–1509.

Dong, P., **Tu, X.**, **Li, H.**, **Zhang, J.**, **Grierson, D.**, **Li, P.** ***et al.*** (2020) Tissue-specific Hi-C analyses of rice, foxtail millet and maize suggest non-canonical function of plant chromatin domains. *Journal of Integrative Plant Biology*, **62**(2), 201–217.

Dong, P., **Tu, X.**, **Liang, Z.**, **Kang, B.H.** & **Zhong, S.** (2020) Plant and animal chromatin three-dimensional organization: similar structures but different functions. *Journal of Experimental Botany*, **71**(17), 5119–5128.

Dong, Q., **Li, N.**, **Li, X.**, **Yuan, Z.**, **Xie, D.**, **Wang, X.** ***et al.*** (2018) Genome-wide Hi-C analysis reveals extensive hierarchical chromatin interactions in rice. *The Plant Journal*, **94**(6), 1141–1156.

Drost, H.G., **Gabel, A.**, **Grosse, I.** & **Quint, M.** (2015) Evidence for active maintenance of phylotranscriptomic hourglass patterns in animal and plant embryogenesis. *Molecular Biology and Evolution*, **32**(5), 1221–1231.

Durand, N.C., **Robinson, J.T.**, **Shamim, M.S.**, **Machol, I.**, **Mesirov, J.P.**, **Lander, E.S.** ***et al.*** (2016) Juicebox provides a visualization system for Hi-C contact maps with unlimited zoom. *Cell Systems*, **3**(1), 99–101.

Durand, N.C., **Shamim, M.S.**, **Machol, I.**, **Rao, S.S.P.**, **Huntley, M.H.**, **Lander, E.S.** ***et al.*** (2016) Juicer provides a one-click system for analyzing loop-resolution Hi-C experiments. *Cell Systems*, **3**(1), 95–98.

Eres, I.E. & **Gilad, Y.** (2021) A TAD skeptic: is 3D genome topology conserved? *Trends in Genetics*, **37**(3), 216–223.

Eres, I.E., **Luo, K.**, **Hsiao, C.J.**, **Blake, L.E.** & **Gilad, Y.** (2019) Reorganization of 3D genome structure may contribute to gene regulatory evolution in primates. *PLoS Genetics*, **15**(7), e1008278. Available from: https://doi.org/10.1371/journal.pgen.1008278

Eser, U., **Chandler-Brown, D.**, **Ay, F.**, **Straight, A.F.**, **Duan, Z.**, **Noble, W.S.** ***et al.*** (2017) Form and function of topologically associating genomic domains in budding yeast. *Proceedings of the National Academy of Sciences of the United States of America*, **114**(15), E3061–E3070.

Farré, M., **Robinson, T.J.** & **Ruiz-Herrera, A.** (2015) An integrative breakage model of genome architecture, reshuffling and evolution. *BioEssays*, **37**(5), 479–488.

Fedoseeva, D.M., **Kretova, O.V.**, **Gorbacheva, M.A.** & **Tchurikov, N.A.** (2018) Individual effects of the copia and gypsy enhancer and insulator on chromatin marks, eRNA synthesis, and binding of insulator proteins in transfected genetic constructs. *Gene*, **641**, 151–160.

Ferguson, A.A., **Zhao, D.** & **Jiang, N.** (2013) Selective acquisition and retention of genomic sequences by pack-utator-like elements based on guanine-cytosine content and the breadth of expression. *Plant Physiology*, **163**(3), 1419–1432.

Fudenberg, G., **Imakaev, M.**, **Lu, C.**, **Goloborodko, A.**, **Abdennur, N.** & **Mirny, L.A.** (2016) Formation of chromosomal domains by loop extrusion. *Cell Reports*, **15**(9), 2038–2049.

Fudenberg, G. & **Pollard, K.S.** (2019) Chromatin features constrain structural variation across evolutionary timescales. *Proceedings of the National Academy of Sciences of the United States of America*, **116**(6), 2175–2180.

Galan, S., **Machnik, N.**, **Kruse, K.**, **Díaz, N.**, **Marti-Renom, M.A.** & **Vaquerizas, J.M.** (2020) CHESS enables quantitative comparison of chromatin contact data and automatic feature extraction. *Nature Genetics*, **52**(11), 1247–1255.

Golicz, A.A., **Bhalla, P.L.**, **Edwards, D.** & **Singh, M.B.** (2020) Rice 3D chromatin structure correlates with sequence variation and meiotic recombination rate. *Communications Biology*, **3**(1), 1–9.

Gorkin, D.U., **Qiu, Y.**, **Hu, M.**, **Fletez-Brant, K.**, **Liu, T.**, **Schmitt, A.D.** ***et al.*** (2019) Common DNA sequence variation influences 3-dimensional conformation of the human genome. *Genome Biology*, **20**(1), 1–25.

Grob, S. & **Grossniklaus, U.** (2017) Chromosome conformation capture-based studies reveal novel features of plant nuclear architecture. *Current Opinion in Plant Biology*, **36**, 149–157.

Groen, S.C., **Ćalić, I.**, **Joly-Lopez, Z.**, **Platts, A.E.**, **Choi, J.Y.**, **Natividad, M.** ***et al.*** (2020) The strength and pattern of natural selection on gene expression in rice. *Nature*, **578**(7796), 572–576.

Groen, S.C., **Joly-Lopez, Z.**, **Platts, A.E.**, **Natividad, M.**, **Fresquez, Z.**, **Mauck, W.M.** ***et al.*** (2022) Evolutionary systems biology reveals patterns of rice adaptation to drought-prone agro-ecosystems. *The Plant Cell*, **34**(2), 759–783.

Gupta, S., **Niels Groen, S.**, **Zaidem, M.L.**, **Sajise, A.G.C.**, **Calic, I.**, **Natividad, M.** ***et al.*** (2025) Systems genomics of salinity stress response in rice. *Elife*, **13**, RP99352.

Gutaker, R.M., **Groen, S.C.**, **Bellis, E.S.**, **Choi, J.Y.**, **Pires, I.S.**, **Bocinsky, R.K.** ***et al.*** (2020) Genomic history and ecology of the geographic spread of rice. *Nature Plants*, **6**(5), 492–502.

Harmston, N., **Ing-Simmons, E.**, **Tan, G.**, **Perry, M.**, **Merkenschlager, M.** & **Lenhard, B.** (2017) Topologically associating domains are ancient features that coincide with metazoan clusters of extreme noncoding conservation. *Nature Communications*, **8**(1), 1–13.

Heinz, S., **Benner, C.**, **Spann, N.**, **Bertolino, E.**, **Lin, Y.C.**, **Laslo, P.** ***et al.*** (2010) Simple combinations of lineage-determining transcription factors prime cis-regulatory elements required for macrophage and B cell identities. *Molecular Cell*, **38**(4), 576–589.

Hinrichs, A.S., **Karolchik, D.**, **Baertsch, R.**, **Barber, G.P.**, **Bejerano, G.**, **Clawson, H.** ***et al.*** (2006) The UCSC genome browser database: update 2006. *Nucleic Acids Research*, **34**(Database issue), D590–D598.

Hisanaga, T., **Wu, S.**, **Schafran, P.**, **Axelsson, E.**, **Akimcheva, S.**, **Dolan, L.** ***et al.*** (2023) The ancestral chromatin landscape of land plants. *The New Phytologist*, **240**(5), 2085–2101.

Hsieh, T.H.S., **Weiner, A.**, **Lajoie, B.**, **Dekker, J.**, **Friedman, N.** & **Rando, O.J.** (2015) Mapping nucleosome resolution chromosome folding in yeast by micro-C. *Cell*, **162**(1), 108–119.

Huynh, L. & **Hormozdiari, F.** (2019) TAD fusion score: discovery and ranking the contribution of deletions to genome structure. *Genome Biology*, **20**(1), 1–13.

Ibn-Salem, J., **Muro, E.M.** & **Andrade-Navarro, M.A.** (2017) Co-regulation of paralog genes in the three-dimensional chromatin architecture. *Nucleic Acids Research*, **45**(1), 81–91.

Ing-Simmons, E., **Vaid, R.**, **Bing, X.Y.**, **Levine, M.**, **Mannervik, M.** & **Vaquerizas, J.M.** (2021) Independence of chromatin conformation and gene regulation during *Drosophila* dorsoventral patterning. *Nature Genetics*, **53**(4), 487–499.

James, C., **Trevisan-Herraz, M.**, **Juan, D.** & **Rico, D.** (2024) Evolutionary analysis of gene ages across TADs associates chromatin topology with whole-genome duplications. *Cell Reports*, **43**(4), 113895.

Jia, J., **Xie, Y.**, **Cheng, J.**, **Kong, C.**, **Wang, M.**, **Gao, L.** ***et al.*** (2021) Homology-mediated inter-chromosomal interactions in hexaploid wheat lead to specific subgenome territories following polyploidization and introgression. *Genome Biology*, **22**(1), 1–21.

Joly-Lopez, Z., **Platts, A.E.**, **Gulko, B.**, **Choi, J.Y.**, **Groen, S.C.**, **Zhong, X.** ***et al.*** (2020) An inferred fitness consequence map of the rice genome. *Nature Plants*, **6**(2), 119–130.

Junaid, A., **Singh, B.** & **Bhatia, S.** (2023) Evolutionary insights into 3D genome organization and epigenetic landscape of *Vigna mungo*. *Life Science Alliance*, **7**(1), e202302074.

Karaaslan, E.S., **Wang, N.**, **Faiß, N.**, **Liang, Y.**, **Montgomery, S.A.**, **Laubinger, S.** ***et al.*** (2020) Marchantia TCP transcription factor activity correlates with three-dimensional chromatin structure. *Nature Plants*, **6**(10), 1250–1261.

Kosugi, S. & **Ohashi, Y.** (2002) DNA binding and dimerization specificity and potential targets for the TCP protein family. *Plant J Cell Mol Biol*, **30**(3), 337–348.

Kou, Y., **Liao, Y.**, **Toivainen, T.**, **Lv, Y.**, **Tian, X.**, **Emerson, J.J.** ***et al.*** (2020) Evolutionary genomics of structural variation in Asian rice (*Oryza sativa*) domestication. *Molecular Biology and Evolution*, **37**(12), 3507–3524.

Krefting, J., **Andrade-Navarro, M.A.** & **Ibn-Salem, J.** (2018) Evolutionary stability of topologically associating domains is associated with conserved gene regulation. *BMC Biology*, **16**(1), 87.

Kruse, K., **Hug, C.B.** & **Vaquerizas, J.M.** (2020) FAN-C: a feature-rich framework for the analysis and visualisation of chromosome conformation capture data. *Genome Biology*, **21**(1), 1–19.

Lazar, N.H., **Nevonen, K.A.**, **O'Connell, B.**, **McCann, C.**, **O'Neill, R.J.**, **Green, R.E.** ***et al.*** (2018) Epigenetic maintenance of topological domains in the highly rearranged gibbon genome. *Genome Research*, **28**(7), 983–997.

Lee, H. & **Seo, P.J.** (2023) Accessible gene borders establish a core structural unit for chromatin architecture in Arabidopsis. *Nucleic Acids Research*, **51**(19), 10261–10277.

Li, D., **He, M.**, **Tang, Q.**, **Tian, S.**, **Zhang, J.**, **Li, Y.** ***et al.*** (2022) Comparative 3D genome architecture in vertebrates. *BMC Biology*, **20**(1), 99.

Li, H. & **Durbin, R.** (2009) Fast and accurate short read alignment with burrows-wheeler transform. *Bioinformatics (Oxford, England)*, **25**(14), 1754–1760.

Liao, Y., **Wang, J.**, **Zhu, Z.**, **Liu, Y.**, **Chen, J.**, **Zhou, Y.** ***et al.*** (2022) The 3D architecture of the pepper genome and its relationship to function and evolution. *Nature Communications*, **13**(1), 1–18.

Liao, Y., **Zhang, X.**, **Chakraborty, M.** & **Emerson, J.J.** (2021) Topologically associating domains and their role in the evolution of genome structure and function in *Drosophila*. *Genome Research*, **31**(3), 397–410. Available from: https://doi.org/10.1101/gr.266130.120

Lieberman-Aiden, E., **van Berkum, N.L.**, **Williams, L.**, **Imakaev, M.**, **Ragoczy, T.**, **Telling, A.** ***et al.*** (2009) Comprehensive mapping of long range interactions reveals folding principles of the human genome. *Science*, **326** (5950), 289–293.

Liu, C., **Cheng, Y.J.**, **Wang, J.W.** & **Weigel, D.** (2017) Prominent topologically associated domains differentiate global chromatin packing in rice from Arabidopsis. *Nature Plants*, **3**(9), 742–748.

Liu, K., **Li, H.**, **Li, Y.**, **Wang, J.** & **Wang, J.** (2022) A comparison of topologically associating domain callers based on Hi-C data. *IEEE/ACM Transactions on Computational Biology and Bioinformatics*, **20**(1), 15–29.

Long, Y., **Liu, Z.**, **Wang, P.**, **Yang, H.**, **Wang, Y.**, **Zhang, S.** ***et al.*** (2021) Disruption of topologically associating domains by structural variations in tetraploid cottons. *Genomics*, **113**(5), 3405–3414.

Madeira, F., **Pearce, M.**, **Tivey, A.R.N.**, **Basutkar, P.**, **Lee, J.**, **Edbali, O.** ***et al.*** (2022) Search and sequence analysis tools services from EMBL-EBI in 2022. *Nucleic Acids Research*, **50**(W1), W276–W279.

Mansueto, L., **Fuentes, R.R.**, **Borja, F.N.**, **Detras, J.**, **Abrio-Santos, J.M.**, **Chebotarov, D.** ***et al.*** (2017) Rice SNP-seek database update: new SNPs, indels, and queries. *Nucleic Acids Research*, **45**(Database issue), D1075.

Marçais, G., **Delcher, A.L.**, **Phillippy, A.M.**, **Coston, R.**, **Salzberg, S.L.** & **Zimin, A.** (2018) MUMmer4: a fast and versatile genome alignment system. *PLoS Computational Biology*, **14**(1), e1005944.

Marchal, C., **Singh, N.**, **Corso-Díaz, X.** & **Swaroop, A.** (2022) HiCRes: a computational method to estimate and predict the genomic resolution of Hi-C libraries. *Nucleic Acids Research*, **50**(6), e35.

McArthur, E. & **Capra, J.A.** (2021) Topologically associating domain boundaries that are stable across diverse cell types are evolutionarily constrained and enriched for heritability. *American Journal of Human Genetics*, **108**(2), 269–283.

Ni, L., **Liu, Y.**, **Ma, X.**, **Liu, T.**, **Yang, X.**, **Wang, Z.** ***et al.*** (2023) Pan-3D genome analysis reveals structural and functional differentiation of soybean genomes. *Genome Biology*, **24**(1), 12.

Nora, E.P., **Lajoie, B.R.**, **Schulz, E.G.**, **Giorgetti, L.**, **Okamoto, I.**, **Servant, N.** ***et al.*** (2012) Spatial partitioning of the regulatory landscape of the X-inactivation centre. *Nature*, **485**(7398), 381–385.

Nuebler, J., **Fudenberg, G.**, **Imakaev, M.**, **Abdennur, N.** & **Mirny, L.A.** (2018) Chromatin organization by an interplay of loop extrusion and compartmental segregation. *Proceedings of the National Academy of Sciences of the United States of America*, **115**(29), E6697–E6706.

Nützmann, H.W., **Doerr, D.**, **Ramírez-Colmenero, A.**, **Sotelo-Fonseca, J.E.**, **Wegel, E.**, **Di Stefano, M.** ***et al.*** (2020) Active and repressed biosynthetic gene clusters have spatially distinct chromosome states. *Proceedings of the National Academy of Sciences of the United States of America*, **117** (24), 13800–13809.

O'Donnell, S. & **Fischer, G.** (2020) MUM&Co: accurate detection of all SV types through whole-genome alignment. *Bioinformatics (Oxford, England)*, **36**(10), 3242–3243.

Okhovat, M., **VanCampen, J.**, **Nevonen, K.A.**, **Harshman, L.**, **Li, W.**, **Layman, C.E.** ***et al.*** (2023) TAD evolutionary and functional characterization reveals diversity in mammalian TAD boundary properties and function. *Nature Communications*, **14**(1), 8111.

Open2C, **Abdennur, N.**, **Fudenberg, G.**, **Flyamer, I.M.**, **Galitsyna, A.A.**, **Goloborodko, A.** ***et al.*** (2023) Pairtools: from sequencing data to chromosome contacts. *bioRxiv* [Preprint Server for Biology] 2023.02.13.528389.

Ou, S., **Su, W.**, **Liao, Y.**, **Chougule, K.**, **Agda, J.R.A.**, **Hellinga, A.J.** ***et al.*** (2019) Benchmarking transposable element annotation methods for creation of a streamlined, comprehensive pipeline. *Genome Biology*, **20**(1), 275.

Pei, L., **Huang, X.**, **Liu, Z.**, **Tian, X.**, **You, J.**, **Li, J.** ***et al.*** (2022) Dynamic 3D genome architecture of cotton fiber reveals subgenome-coordinated chromatin topology for 4-staged single-cell differentiation. *Genome Biology*, **23**(1), 45.

Pockrandt, C., **Alzamel, M.**, **Iliopoulos, C.S.** & **Reinert, K.** (2020) GenMap: ultra-fast computation of genome mappability. *Bioinformatics (Oxford, England)*, **36**(12), 3687–3692.

Prieto, P., **Santos, A.P.**, **Moore, G.** & **Shaw, P.** (2004) Chromosomes associate premeiotically and in xylem vessel cells via their telomeres and centromeres in diploid rice (*Oryza sativa*). *Chromosoma*, **112**(6), 300–307.

Quinlan, A.R. & **Hall, I.M.** (2010) BEDTools: a flexible suite of utilities for comparing genomic features. *Bioinformatics (Oxford, England)*, **26**(6), 841–842.

Ramírez, F., **Bhardwaj, V.**, **Arrigoni, L.**, **Lam, K.C.**, **Grüning, B.A.**, **Villaveces, J.** ***et al.*** (2018) High-resolution TADs reveal DNA sequences underlying genome organization in flies. *Nature Communications*, **9**(1), 189.

Ramírez, F., **Ryan, D.P.**, **Grüning, B.**, **Bhardwaj, V.**, **Kilpert, F.**, **Richter, A.S.** ***et al.*** (2016) deepTools2: a next generation web server for deep-sequencing data analysis. *Nucleic Acids Research*, **44**(W1), W160–W165.

Rao, S.S.P., **Huntley, M.H.**, **Durand, N.C.**, **Stamenova, E.K.**, **Bochkov, I.D.**, **Robinson, J.T.** ***et al.*** (2014) A 3D map of the human genome at kilobase resolution reveals principles of chromatin looping. *Cell*, **159**(7), 1665–1680.

Renschler, G., **Richard, G.**, **Valsecchi, C.I.K.**, **Toscano, S.**, **Arrigoni, L.**, **Ramírez, F.** ***et al.*** (2019) Hi-C guided assemblies reveal conserved regulatory topologies on X and autosomes despite extensive genome shuffling. *Genes & Development*, **33**(21–22), 1591–1612.

Robinson, M.D., **McCarthy, D.J.** & **Smyth, G.K.** (2010) edgeR: a bioconductor package for differential expression analysis of digital gene expression data. *Bioinformatics (Oxford, England)*, **26**(1), 139–140.

Rowley, M.J., **Nichols, M.H.**, **Lyu, X.**, **Wang, P.**, **Ruan, Y.**, **Corces, V.G.** ***et al.*** (2017) Evolutionarily conserved principles predict 3D article evolutionarily conserved principles predict 3D chromatin organization. *Molecular Cell*, **67**, 837–852.

Schmidbaur, H., **Kawaguchi, A.**, **Clarence, T.**, **Fu, X.**, **Hoang, O.P.**, **Zimmermann, B.** ***et al.*** (2022) Emergence of novel cephalopod gene regulation and expression through large-scale genome reorganization. *Nature Communications*, **13**(1), 2172.

Shao, W., **Wang, J.**, **Zhang, Y.**, **Zhang, C.**, **Chen, J.**, **Chen, Y.** ***et al.*** (2024) The jet-like chromatin structure defines active secondary metabolism in fungi. *Nucleic Acids Research*, **52**, 4906–4921.

Stein, J.C., **Yu, Y.**, **Copetti, D.**, **Zwickl, D.J.**, **Zhang, L.**, **Zhang, C.** ***et al.*** (2018) Genomes of 13 domesticated and wild rice relatives highlight genetic conservation, turnover and innovation across the genus *Oryza*. *Nature Genetics*, **50**(2), 285–296.

Sun, L., **Zhou, J.**, **Xu, X.**, **Liu, Y.**, **Ma, N.**, **Liu, Y.** ***et al.*** (2024) Mapping nucleosome-resolution chromatin organization and enhancer-promoter loops in plants using micro-C-XL. *Nature Communications*, **15**(1), 1–18.

Szabo, Q., **Jost, D.**, **Chang, J.M.**, **Cattoni, D.I.**, **Papadopoulos, G.L.**, **Bonev, B.** ***et al.*** (2018) TADs are 3D structural units of higher-order chromosome organization in *Drosophila*. *Science Advances*, **4**(2), eaar8082. Available from: https://doi.org/10.1126/sciadv.aar8082

Tian, L., **Ku, L.**, **Yuan, Z.**, **Wang, C.**, **Su, H.**, **Wang, S.** ***et al.*** (2021) Large-scale reconstruction of chromatin structures of maize temperate and tropical inbred lines. *Journal of Experimental Botany*, **72**(10), 3582–3596.

Torosin, N.S., **Anand, A.**, **Golla, T.R.**, **Cao, W.** & **Ellison, C.E.** (2020) 3D genome evolution and reorganization in the *Drosophila melanogaster* species group. *PLoS Genetics*, **16**(12), e1009229.

Torosin, N.S., **Golla, T.R.**, **Lawlor, M.A.**, **Cao, W.** & **Ellison, C.E.** (2022) Mode and tempo of 3D genome evolution in *Drosophila*. *Molecular Biology and Evolution*, **39**(11), msac216.

Torres, D.E., **Kramer, H.M.**, **Tracanna, V.**, **Fiorin, G.L.**, **Cook, D.E.**, **Seidl, M.F.** ***et al.*** (2024) Implications of the three-dimensional chromatin organization for genome evolution in a fungal plant pathogen. *Nature Communications*, **15**(1), 1701.

Tourdot, E. & **Grob, S.** (2023) Three-dimensional chromatin architecture in plants – general features and novelties. *European Journal of Cell Biology*, **102**(4), 151344.

Vietri Rudan, M., **Barrington, C.**, **Henderson, S.**, **Ernst, C.**, **Odom, D.T.**, **Tanay, A.** ***et al.*** (2015) Comparative Hi-C reveals that CTCF underlies evolution of chromosomal domain architecture. *Cell Reports*, **10**(8), 1297–1309.

Wang, M., **Li, J.**, **Wang, P.**, **Liu, F.**, **Liu, Z.**, **Zhao, G.** ***et al.*** (2021) Comparative genome analyses highlight transposon-mediated genome expansion and the evolutionary architecture of 3D genomic folding in cotton. *Molecular Biology and Evolution*, **38**(9), 3621–3636.

Wang, M., **Wang, P.**, **Lin, M.**, **Ye, Z.**, **Li, G.**, **Tu, L.** ***et al.*** (2018) Evolutionary dynamics of 3D genome architecture following polyploidization in cotton. *Nature Plants*, **4**(2), 90–97.

Wang, X.T., **Cui, W.** & **Peng, C.** (2017) HiTAD: detecting the structural and functional hierarchies of topologically associating domains from chromatin interactions. *Nucleic Acids Research*, **45**(19), e163.

Wu, T., **Hu, E.**, **Xu, S.**, **Chen, M.**, **Guo, P.**, **Dai, Z.** ***et al.*** (2021) clusterProfiler 4.0: a universal enrichment tool for interpreting omics data. *Innovation (Cambrdige, Mass.)*, **2**(3), 100141.

Xia, C., **Huang, L.**, **Huang, J.**, **Zhang, H.**, **Huang, Y.**, **Benhamed, M.** ***et al.*** (2022) Folding features and dynamics of 3D genome architecture in plant fungal pathogens. *Microbiology Spectrum*, **10**(6), e0260822.

Xie, T., **Zhang, F.G.**, **Zhang, H.Y.**, **Wang, X.T.**, **Hu, J.H.** & **Wu, X.M.** (2019) Biased gene retention during diploidization in *Brassica* linked to three-dimensional genome organization. *Nature Plants*, **5**(8), 822–832.

Xu, W., **Zhong, Q.**, **Lin, D.**, **Zuo, Y.**, **Dai, J.**, **Li, G.** ***et al.*** (2021) CoolBox: a flexible toolkit for visual analysis of genomics data. *BMC Bioinformatics*, **22** (1), 1–9.

Yang, T., **Zhang, F.**, **Yardımcı, G.G.**, **Song, F.**, **Hardison, R.C.**, **Noble, W.S.** ***et al.*** (2017) HiCRep: assessing the reproducibility of Hi-C data using a stratum-adjusted correlation coefficient. *Genome Research*, **27**(11), 1939–1949. Available from: https://doi.org/10.1101/gr.220640.117

Yin, X., **Romero-Campero, F.J.**, **Yang, M.**, **Baile, F.**, **Cao, Y.**, **Shu, J.** ***et al.*** (2023) Binding by the Polycomb complex component BMI1 and H2A monoubiquitination shape local and long-range interactions in the Arabidopsis genome. *The Plant Cell*, **35**(7), 2484–2503.

Young, M.D., **Willson, T.A.**, **Wakefield, M.J.**, **Trounson, E.**, **Hilton, D.J.**, **Blewitt, M.E.** ***et al.*** (2011) ChIP-seq analysis reveals distinct H3K27me3 profiles that correlate with transcriptional activity. *Nucleic Acids Research*, **39**(17), 7415–7427.

Zhan, Y., **Mariani, L.**, **Barozzi, I.**, **Schulz, E.G.**, **Blüthgen, N.**, **Stadler, M.** ***et al.*** (2017) Reciprocal insulation analysis of Hi-C data shows that TADs represent a functionally but not structurally privileged scale in the hierarchical folding of chromosomes. *Genome Research*, **27**(3), 479–490.

Zhang, L., **Zhao, J.**, **Bi, H.**, **Yang, X.**, **Zhang, Z.**, **Su, Y.** ***et al.*** (2021) Bioinformatic analysis of chromatin organization and biased expression of duplicated genes between two poplars with a common whole-genome duplication. *Horticulture Research*, **8**(1), 1–12.

Zhang, R.G., **Li, G.Y.**, **Wang, X.L.**, **Dainat, J.**, **Wang, Z.X.**, **Ou, S.** ***et al.*** (2022) TEsorter: an accurate and fast method to classify LTR-retrotransposons in plant genomes. *Horticulture Research*, **9**, uhac017.

Zhang, X., **Pandey, M.K.**, **Wang, J.**, **Zhao, K.**, **Ma, X.**, **Li, Z.** ***et al.*** (2021) Chromatin spatial organization of wild type and mutant peanuts reveals high-resolution genomic architecture and interaction alterations. *Genome Biology*, **22**(1), 1–21.

Zhang, X. & **Wang, T.** (2021) Plant 3-D chromatin organization: important insights from chromosome conformation capture analyses of the last 10 years. *Plant & Cell Physiology*, **62**(11), 1648–1661.

Zhao, L., **Wang, S.**, **Cao, Z.**, **Ouyang, W.**, **Zhang, Q.**, **Xie, L.** ***et al.*** (2019) Chromatin loops associated with active genes and heterochromatin shape rice genome architecture for transcriptional regulation. *Nature Communications*, **10**(1), 1–13.

Zhao, L., **Xie, L.**, **Zhang, Q.**, **Ouyang, W.**, **Deng, L.**, **Guan, P.** ***et al.*** (2020) Integrative analysis of reference epigenomes in 20 rice varieties. *Nature Communications*, **11**(1), 1–16.

Zhou, S., **Jiang, W.**, **Zhao, Y.** & **Zhou, D.X.** (2019) Single-cell three-dimensional genome structures of rice gametes and unicellular zygotes. *Nature Plants*, **5**(8), 795–800.

Zhou, Y., **Zhan, X.**, **Jin, J.**, **Zhou, L.**, **Bergman, J.**, **Li, X.** ***et al.*** (2023) Eighty million years of rapid evolution of the primate Y chromosome. *Nature Ecology & Evolution*, **7**(7), 1114–1130.

Zufferey, M., **Tavernari, D.**, **Oricchio, E.** & **Ciriello, G.** (2018) Comparison of computational methods for the identification of topologically associating domains. *Genome Biology*, **19**(1), 1–18.